Czech Technical University in Prague
Faculty of Electrical Engineering
Department of Telecommunication Engineering

Deployment of flying base stations in emergency situations

Diploma thesis

Bc. Tomáš Sap

Study programme: Electronics and communication
Field of study: Mobile communication
Supervisor: doc. Ing. Zdeněk Bečvář, Ph.D.

Prague, May 2022

Thesis Supervisor:
doc. Ing. Zdeněk Bečvář, Ph.D.
Department of Telecommunication Engineering
Faculty of Electrical Engineering
Czech Technical University in Prague
Technická 2
160 00 Prague 6
Czech Republic

MASTER'S THESIS ASSIGNMENT

I. Personal and study details

Student's name: **Sap Tomáš** Personal ID number: **474250**

Faculty / Institute: **Faculty of Electrical Engineering**

Department / Institute: **Department of Telecommunications Engineering**

Study program: **Electronics and Communications**

Specialisation: **Mobile Communications**

II. Master's thesis details

Master's thesis title in English:

Deployment of Flying Base Stations in Emergency Situations

Master's thesis title in Czech:

Rozmístění létajících základnových stanic pro mimořádné události

Guidelines:

Study concept of flying base stations for future mobile networks, i.e., base stations mounted on unmanned aerial vehicles (UAVs). Propose an algorithm determining positions of the flying base station so that user can communicate in real-time during emergency situations. Consider connection of the flying base stations to core network including multi-hop relaying via intermediate flying base stations. Test efficiency of the proposed solution via simulations.

Bibliography / sources:

[1] P. Mach, Z. Becvar, M. Najla, 'Power Allocation, Channel Reuse, and Positioning of Flying Base Stations with Realistic Backhaul', IEEE Internet of Things Journal, 2021.
[2] M. Nikooroo, Z. Becvar, 'Optimal Positioning of Flying Base Stations and Transmission Power Allocation in NOMA Networks', IEEE Transactions on Wireless Communications, 2021.
[3] A. Fouda, A. S. Ibrahim, I. Guvenc, and M. Ghosh, "Interference Management in UAV-Assisted Integrated Access and Backhaul Cellular Networks," IEEE Access, Vol. 7, 2019.
[4] Y. Li, G. Feng, M. Ghasemiahmadi, and L. Cai, "Power Allocation and 3-D Placement for Floating Relay Supporting Indoor Communications," IEEE Trans. Mobile Comput., vol. 18, no. 3, pp. 618-631, 2018.

Name and workplace of master's thesis supervisor:

doc. Ing. Zdeněk Bečvář, Ph.D. Department of Telecommunications Engineering FEE

Name and workplace of second master's thesis supervisor or consultant:

Date of master's thesis assignment: **21.01.2022** Deadline for master's thesis submission: **20.05.2022**

Assignment valid until: **30.09.2023**

doc. Ing. Zdeněk Bečvář, Ph.D. Supervisor's signature	Head of department's signature	prof. Mgr. Petr Páta, Ph.D. Dean's signature

III. Assignment receipt

The student acknowledges that the master's thesis is an individual work. The student must produce his thesis without the assistance of others, with the exception of provided consultations. Within the master's thesis, the author must state the names of consultants and include a list of references.

Date of assignment receipt	Student's signature

Declaration

I hereby declare I have written this diploma thesis independently and quoted all the sources of information used in accordance with methodological instructions on ethical principles for writing an academic thesis. Moreover, I state that this thesis has neither been submitted nor accepted for any other degree.

In Prague, May 2022

.....
Bc. Tomáš Sap

Abstract

In general emergency scenarios like natural or other disasters, a highly flexible network providing reliable connectivity to all critical users within the disaster area is crucial for successful search and rescue. Therefore, as in such scenario it is not possible to classify individual users in terms of urgency, it is important to secure sufficient capacity for each of them. To provide a scalable and flexible radio access network suitable for emergency scenarios, the utilization of mobile flying base stations (FlyBS), which forward communication between the users and the network, has already been proposed in recent research. However, the majority of the works focus only on the sum capacity maximization, neglecting the users with low channel quality. Thus, to address the sufficient capacity requirement, a framework for FlyBS deployment that maximizes the minimal channel capacity among all users in the cell is proposed in this thesis. The framework adopts a novel power allocation scheme that equalizes end-to-end channel capacities among all the user equipments (UEs), and at the same time, finds the FlyBS positions and UE associations jointly via a proposed heuristic algorithm. The results of the final simulations show that the proposed scheme significantly increases the minimal channel capacity compared to the competitive schemes, and that is by approximately 53% – 244% based on the varying number of UEs and FlyBSs in the cell. However, this is achieved at the cost of sum capacity, which decreases by about 5% – 30% due to limited power resources.

Keywords: mobile network, flying base station, emergency scenarios, minimal capacity, power allocation, positioning of FlyBSs, association of users

Abstrakt

V mimořádných situacích, jako jsou přírodní či jiné katastrofy, je zajištění flexibilního a spolehlivého mobilního připojení pro všechny uživatele nacházející se v zasažené oblasti klíčovým prvkem pro úspěšnost záchranných akcí. Jelikož není v takové situaci obecně možné klasifikovat uživatele na základě důležitosti či hrozícího nebezpečí, je nezbytné zajistit dostatečnou přenosovou kapacitu pro všechny uživatele bez výjimky. Za účelem zajištění dostatečně flexibilní přístupové sítě vhodné pro mimořádné situace je zkoumána především možnost nasazení létajících základnových stanic (FlyBS), jejichž úkolem je přepojovat komunikaci mezi uživateli a páteřní sítí. Nicméně, většina dosavadního výzkumu se zaměřuje především na maximalizaci celkové kapacity, což je v případě mimořádných událostí nevhodné, jelikož tak dochází k zanedbávání uživatelů s horší kvalitou kanálu. Tato práce za účelem zajištění dostatečné a férové přenosové kapacity navrhuje způsob nasazení létajících základnových stanic v konvenční buňkové síti, který zajišťuje maximalizaci minimální kapacity mezi všemi uživateli (UE). Navržené řešení alokuje vysílací výkon pro všechny spoje v rámci buňky tak, aby byla výsledná kapacita pro všechny UE stejná, a zároveň představuje algoritmus, který na základě této alokace hledá vhodné polohy FlyBS a asociaci UE. Finální simulace ukazují, že v maximalizaci minimální kapacity návrh výrazně překonává všechny konkurenční řešení, a to téměř o 53% – 244% v závislosti na různých počtech UE a FlyBS v buňce. Nicméně, tohoto výsledku je dosaženo za cenu celkové kapacity buňky, která tímto klesá přibližně o 5% – 30% z důvodu omezení celkového dostupného výkonu.

Klíčová slova: mobilní síť, létající základnová stanice, mimořádné události, minimální kapacita, alokace výkonu, polohování FlyBS, asociace uživatelů

Acknowledgements

First and foremost, I would like to express my gratitude to doc. Ing. Zdeněk Bečvář, Ph.D, for his supervision, invaluable advice, and assistance with every stage of the thesis. My appreciation also goes out to my family and especially my girlfriend for their continuous support, encouragement, and belief in me.

List of Tables

List of Figures

List of Abbreviations

BS	Base Station
FlyBS	Flying Base Station
UE	User Equipment
SINR	Signal to Interference and Noise Ratio
RAN	Radio Access Network
QoS	Quality of Service

Contents

Chapter 1

Introduction

For future mobile networks, a constant rise in throughput requirements and demand for radio access network versatility is expected [1]. This trend, in the long term, results in a constant development leading to deployment of new technology generation approximately every 10 years. As the throughput is mainly linked to the utilized bandwidth, this evolution gradually increases occupancy of the available band, which especially for the last generation leads to the utilization of much higher, millimeter-wave bands [2], resulting in a significant coverage loss [3]. This effect naturally calls for dense deployment of small cells, which not only increases the expenditure of the network's implementation but also introduces problems for mobility management [4], as higher the intensity of handovers has to be taken into account.

Other issues not fully addressed by today's generation of mobile networks are the coverage of remote areas, where due to economical or geographical limitations a cell cannot be deployed, and irregular overloading of individual cells during special occasions. These can be social events, emergency situations, or traffic jams, where the intensity of users' demand within one or several cells increases temporarily and irregularly. Thus, this problem cannot be effectively addressed by dimensioning the ground network.

For all of the presented issues, a base station integrated onto an unmanned aerial vehicle (UAV) is emerging as a promising solution [5]. This flying base station (FlyBS) serves as a mobile relay station that forwards communication between a user equipment (UE) and a ground base station (GBS), thus extending the backhaul and moving the access network closer to the particular point of current access demand. Then, this highly scalable and flexible cellular network supported by mobile FlyBSs could quickly and autonomously adapt to a wide range of scenarios [5]. For example, the FlyBSs would allow an increase in coverage of remote areas [6][7][8], mitigate cell overloading by supplying FlyBSs from surrounding less loaded cells [9][10], or improve connectivity to a high number of users moving in a crowd in areas, where the dense deployment of small cells is not economical

[5][11]. Last but not least, in emergency scenarios, deployment of the FlyBSs could provide a fast recovery of a damaged ground network, or a high capacity flexible connectivity, where effective and reliable communication among emergency services is needed [12].

Nevertheless, implementation of the FlyBS-supported network faces various challenges, such as optimal deployment and positioning of introduced flying base stations, an association of UEs with these FlyBSs, and effective allocation of bandwidth and power resources [13]. Association and UAV positioning problems are addressed jointly in a majority of works, such as [14][15][16][17] and [18]. However, most of these do not take the backhaul communication between the FlyBS and the serving GBS into account, thus neglecting the intergration of the FlyBSs into the ground cellular network. This is a major drawback, as firstly, the FlyBS cannot provide connectivity to ground users without a backhaul connection to the core network, and secondly, the backhaul has a significant impact on the performance of access network between the FlyBS and associated UEs. This impact is lower when different frequency resources are allocated for access and backhaul, as those links do not interfere with each other. However, this is highly inefficient in terms of spectral utilization, especially in cases where the majority of users in the cell are connected to the FlyBSs.

To address this issue, allocation of the same spectral resources to both access and backhaul is introduced in [19]. Then, the same approach is further improved in [20], which proposes a backhaul-aware association of UEs to either the BS or one of the FlyBSs based on offered channel capacity. The association is evaluated jointly with the power allocation. At each FlyBS, the power is allocated to individual associated UEs to match the capacity at access with the backhaul capacity. Otherwise, one of the two links would serve as a bottleneck, making the other one unnecessarily waste power resources. The positions of FlyBSs are then corrected to utilize their whole available power budget. Although the solution is power efficient and achieves higher capacities, it still suffers from limited flexibility, as the power allocated at the BS is the same for all backhaul links and all UEs directly associated with the BS. Another promising solution to FlyBS positioning is described in [21], where the authors, inspired by the Coulomb's law, propose positioning via virtual attraction and repulsion forces analogous to electrostatic forces between charged particles. The solution is highly power-efficient, however, it again considers static power allocation for all UEs, limiting the flexibility of the network.

All of the above-mentioned solutions mainly focus on maximization of sum channel capacity and do not take requirements of individual FlyBS deployment use cases into account. In emergency scenarios, such as natural disasters like earthquakes, floods, and hurricanes, providing reliable connectivity is crucial for search and rescue. Therefore, it is important to secure sufficient capacity for each and every UE in the critical zone, be

it a member of emergency services or a person in distress. This requirement naturally calls for the maximization of minimal capacity among the UEs. Neither of the above-presented schemes serves as a suitable solution, as the maximization of sum capacity naturally results in neglecting certain users with low channel quality. Deployment of FlyBSs in emergency scenarios is addressed in [22], where the FlyBS is dedicated to each couple of users. However, this results in the deployment of a high unrealistic number of FlyBSs. Then, an improved framework for UAV-assisted emergency networks is proposed in [23]. The solution considers a damaged BS substituted by the FlyBS, that forwards the communication to a neighboring cell via a multihop FlyBS relay. However, the throughput of such network is really low, as firstly, only one FlyBS is used to serve the whole discontinued cell, and secondly, the spectral resources are split among individual links of the multihop relay, further decreasing the capacity. In addition, an optimal power allocation among multiple FlyBSs, based on both path loss and fading, is described in [24]. Nevertheless, although the proposed allocation is very accurate, it primarily addresses post-disaster network restoration to provide demanded QoS to users no longer in danger. Therefore, its purpose is only to maximize the sum capacity, neglecting fairness among users.

Considering a general emergency scenario with the above-specified requirements, the objective of this thesis is to maximize the minimal channel capacity among all UEs, via association of users, power allocation, and positioning of the FlyBSs relaying data from the network to the users. The contributions of this work are summarized as follows:

- An expression for optimal power allocation maximizing the minimal capacity for a given association and positioning configuration is derived. The proposed scheme maximizes the minimal capacity via allocating the power in a way, that all UEs experience the same end-to-end channel capacity while utilizing most of the available power. This is achieved via the determination of transmission powers for all links, including also backhaul of the FlyBSs and direct links between the UEs and the BS, contrary to the works mentioned above.

- An effective initial association scheme, that considers both the FlyBSs and the BS, is proposed. The scheme is based on modified *k-means* clustering, which associates the UEs to either one of the FlyBSs or the BS, achieving an effective distribution of available transmission power.

- A joint power-efficient FlyBS positioning and association correction is proposed. The solution utilizes the above-mentioned power allocation together with partial positioning and association schemes to converge to a final stable configuration. To

save time and resources, the proposed scheme is designed to be executed virtually until a final configuration is obtained.

- Via final simulations, it is demonstrated that the designed solution outperforms the examined competitive schemes in maximization of minimal capacity by up to 244%.
- Possibility of integration of the FlyBS multihop relay utilizing the same resources for each link is examined in a simplified scenario. The simulation results show that the multihop is beneficial only to a limited number of utilized FlyBSs in terms of capacity gain. Furthermore, this number depends on the carrier frequency and the total distance the multihop covers.

To introduce the proposed solution, first, the system model describing the environment and mutual relations among network objects is described in Chapter 2. Then, in Chapter 3, the proposed power allocation scheme maximizing the minimal capacity together with algorithms handling the FlyBS positioning and UE's association is outlined. Consequently, in Chapter 4, the performance of the established network in various scenarios and system configurations is evaluated via simulations. Finally, the thesis is concluded in Chapter 5, where the final results and possible future research directions are presented.

Chapter 2

System model and problem formulation

In this chapter, the system model with its parameters and key internal relations is described, and then, the problem addressed in this thesis is formulated.

2.1 System model

In this section, the whole system model considered in this thesis is described. First, the system space, system objects, and relations between them are established. Then, parameters and quantities describing signal propagation and communication channels are defined.

2.1.1 System space

In the system model, a multicell scenario is considered. A reference cell of $\mathbb{R}^2$ dimensions $x_c \times y_c$ is surrounded by N_I neighboring cells, each managed by a base station v, where $v \in \mathbb{B}_I = \{1, ..., N_I\}$, serving as an interference source. In the reference cell, objects of three types are considered: a serving base station (BS), N_{FlyBS} flying base stations given by the set $\mathcal{F} = \{f_1, f_2, ..., f_{N_{FlyBS}}\}$ and N_{UE} UEs defined by the set $\mathcal{U} = \{u_1, u_2, ..., u_{N_{UE}}\}$. Then, $\mathbb{F} = \{1, ..., N_{FlyBS}\}$ is a set of FlyBS indices and similarly $\mathbb{U} = \{1, ..., N_{UE}\}$ is a set of UE indices. As both BS and FlyBS are system objects dedicated to serving the UEs, they are generally denoted as *serving stations* in this thesis.

Positions of objects are generally $\mathbb{R}^3$. Each is defined by cartesian x, y, z coordinates, where x and y are generally free. The z coordinate, being an altitude of a radio communication interface above the x, y plane, is fixed and given by a constant value defined for each object type separately, that is z_{BS}, z_{FlyBS}, and z_{UE} for the BS, FlyBS and UE respectively. The position of the reference cell's BS r_{bs} is constant and fixed

at $\{x_c/2, y_c/2, z_{BS}\}$, that is the middle of the cell. Then, positions of UEs and FlyBSs are free in $\mathbb{R}^2$, restricted only by the dimensions of the reference cell. Positions of UEs $r_{ue,i}$, where $i \in \mathbb{U}$, are considered independent. On the other hand, positions $r_{flybs,j}$ of all FlyBSs $j \in \mathbb{F}$ are variables dependent on the state of the system and define a set of FlyBS positions $\boldsymbol{R} = \{r_{flybs,1}, ..., r_{flybs,N_{FlyBS}}\}$.

2.1.2 Relations between system objects

As the purpose of the cellular network is to provide connectivity of end users to the core network, all UEs have to be connected to the BS either directly or via one of the FlyBSs. In the system model, this is provided via associations between system objects, which form a spanning tree with the BS as its center. The associations denote a direction, in which the downlink communication is forwarded. Hence, if a particular UE is associated with the BS, downlink communication is forwarded directly from the BS to that UE. Such association is called a *direct link* in the system. If the UE is associated with one of the FlyBSs and the FlyBS is then associated with the BS, the downlink communication if forwarded via the FlyBS, which serves as a relay station between the UE and the BS. Such configuration is called a *relay link*, where a connection between UE and FlyBS is denoted as *access link* and connection between FlyBS and BS as *backhaul link* [25].

However, in case of the relay link, the FlyBS does not have to necessarily be associated with the BS. In general, the FlyBS can be associated with another FlyBS forming a *multihop relay*, provided that the whole relay link is terminated at the BS. The multihop relay is then formed by a general number of N_R interconnected FlyBSs. An established system model with an example of possible associations is illustrated in Figure 2.1.

Associations between the FlyBSs and the BS, as well as among FlyBSs forming the multihop together, are fixed and cannot change. On the other hand, associations of the UEs with the serving stations are dynamic and subject to the state of the system. Each UE can be associated only with a single serving station at a time. The same applies also to associations of the FlyBSs in direction to the BS. Associations in the system are managed in a decentralized manner. Each UE i and FlyBS j holds a set, $\boldsymbol{a_i}$ and $\boldsymbol{a_j^{(F)}}$ respectively, defining which serving station the object is associated with and which not. Thus, the association sets are defined as:

$$\begin{aligned} \boldsymbol{a_i} &= \left\{a_{i,b}, a_{i,1}, ..., a_{i,l}, a_{i,l+1}, ..., a_{i,N_{FlyBS}}\right\}, \\ \boldsymbol{a_j^{(F)}} &= \left\{a_{j,b}^{(F)}, a_{j,1}^{(F)}, ..., a_{j,l}^{(F)}, a_{j,l+1}^{(F)}, ..., a_{j,N_{FlyBS}}^{(F)}\right\}, \end{aligned} \tag{2.1}$$

where the first element in both sets denotes association with the BS, and the rest determines association with FlyBS $l \in \{1, ..., N_{FlyBS}\}$. Therefore, the individual elements are defined as:

$$a_{i,b}, a_{j,b}^{(F)} = \begin{cases} 1, & \text{if UE } i \text{ or FlyBS } j \text{ is associated with the BS,} \\ 0, & \text{otherwise.} \end{cases},$$
$$a_{i,l}, a_{j,l}^{(F)} = \begin{cases} 1, & \text{if UE } i \text{ or FlyBS } j \text{ is associated with FlyBS } l, \\ 0, & \text{otherwise.} \end{cases}. \tag{2.2}$$

Then, the defined association sets $\boldsymbol{a_i}$ and $\boldsymbol{a_j^{(F)}}$ form an association matrix of the system $\boldsymbol{A} = \{\boldsymbol{a_1}, ..., \boldsymbol{a_{N_{UE}}}, \boldsymbol{a_1^{(F)}}, ..., \boldsymbol{a_{N_{FlyBS}}^{(F)}}\}$, that describes all associations in the model. In addition to that, each serving station maintains a list of UEs associated with it. The list is given by a set of associated UEs' indices and is denoted as $\mathbb{U}_j^{(F)}$ in case of FlyBS j, and similarly, $\mathbb{U}_B$ is the case of the BS.

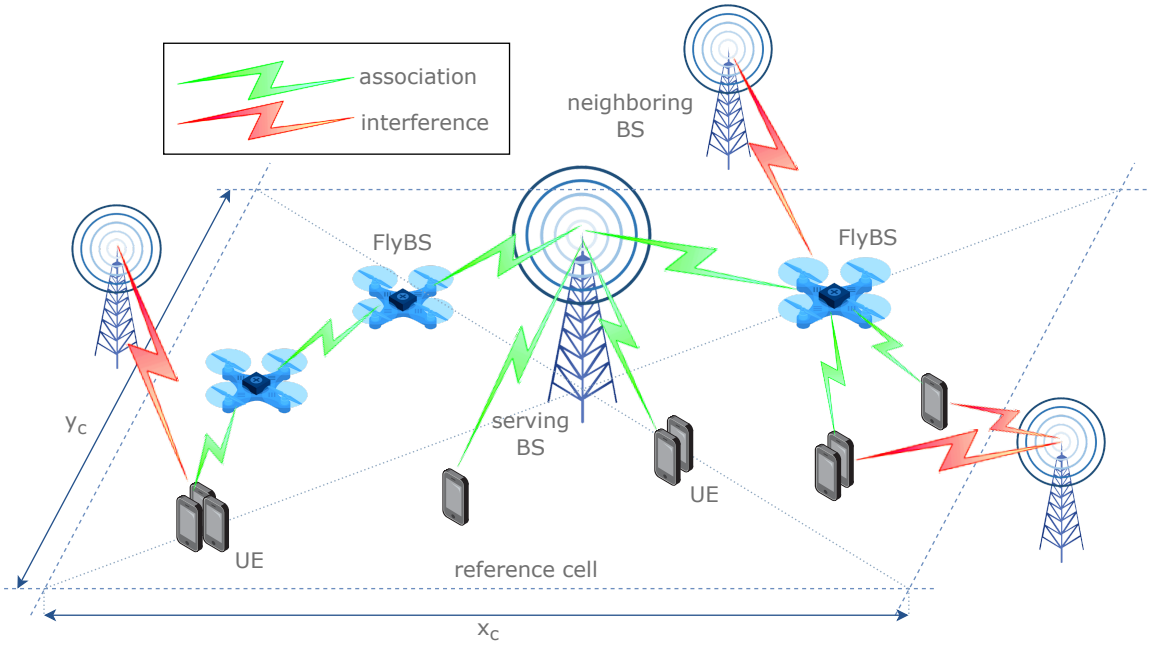

Figure 2.1: Illustrative example of system model with possible associations

2.1.3 Bandwidth management

The bandwidth allocation is managed by each BS separately, while all cells, that is both the reference and the neighboring cells, operate on the same frequency band and share the same bandwidth B. Within the reference cell, the bandwidth is equally distributed among all served UEs, e.i., the bandwidth B_{UE} allocated to each UE is:

$$B_{UE} = \frac{B}{N_{UE}}. \tag{2.3}$$

Then, the allocated channel with bandwidth B_{UE} is used for the whole communication between certain UE and the BS. Furthermore, to increase the spectrum efficiency, the channel is shared between the *access* and *backhaul* links in case of the relayed communication, as in [19][20] and [26].

The neighboring cells serve only as sources of interference to the reference cell. Therefore, it is sufficient to estimate their bandwidth allocation based on the reference cell. It is considered that each of the neighboring cells serves the same amount of N_{UE} UEs as the reference, and thus, allocates the same bandwidth B_{UE} to all of them. Then, each communication link in the reference cell is interfered by each of the neighboring BSs on the whole width of the utilized channel.

2.1.4 Transmission power management

The power that can be allocated for downlink transmission on the serving station is limited by a dedicated total power budget, which is denoted as P_B in the case of the BS, and P_F in the case of the FlyBS. Then, p_i is the power allocated for UE i, and similarly, $p_j^{(F)}$ is the power allocated for FlyBS j regardless of the association. Finally, the system power allocation set is defined as $\boldsymbol{P} = \{p_1, ..., p_{N_{UE}}, p_1^{(F)}, ..., p_{N_{FlyBS}}^{(F)}\}$, where each element is a dynamic variable subject to the state of the system. Additionally, as the inner configuration of the neighboring cells is not relevant, the transmission power allocated for all channels in the neighboring cells is defined as:

$$p_I = \frac{P_B}{N_{UE}}. \tag{2.4}$$

2.1.5 Channel gain

In the system model, a line-of-sight (LoS) environment is considered for all communication links. Therefore, based on the free-space path loss model, the gain of the channel between general system objects m and n is defined as:

$$g_{m,n} = \left(\frac{v}{4\pi d_{m,n} f}\right)^2, \tag{2.5}$$

where v is the radio wave propagation speed, $d_{m,n}$ is Euclidean distance between objects m and n, and finally, f is the communication frequency.

Given the LoS environment, the evaluated channel gain serves as a substitution for gain, that would be actually measured in a real network. However, measurement of the

gain is not always available. To overcome this, a path loss prediction method described in [27][28] is utilized in such situation. As the evaluation is burdened with a prediction error according to [27], the predicted gain is in the model simulated as:

$$g_{m,n}^{(p)} = \left(\frac{v}{4\pi d_{m,n} f}\right)^2 \cdot 10^{\frac{\Phi}{10}}, \tag{2.6}$$

where Φ is the path loss prediction error in dB.

2.1.6 Interference

In the system model, two types of interference are defined: *inter-cell*, caused by the surrounding base stations, and *intra-cell*, caused by the objects within the reference cell. The inter-cell interference is given by the sum of contributions from each of the surrounding base stations, while the intra-cell interference is given by the sum of contributions from objects within the cell that use the same spectral resources, and thus affects only relay links [20][26].

Hence, the SINR of the direct BS to UE i downstream link obtained at the UE's downlink radio interface is expressed as:

$$SINR_i^{(D)} = \frac{p_i g_{i,b}}{\sigma B_{UE} + \sum_{v \in \mathbb{B}_I} p_I g_{i,v}}, \tag{2.7}$$

where p_i is the downlink transmission power allocated to UE i, p_I is the transmission power of an interfering signal, B_{UE} is the bandwidth allocated to UE i, and σ is the noise spectral density. Finally, the parameters $g_{i,b}$ and $g_{i,v}$ stand for channel gain between the UE i and the serving BS, and UE i and neighboring BS v, respectively.

Considering a simple relayed communication via a single FlyBS, a similar equation to (2.7) applies also for SINR of the backhaul BS to FlyBS j downstream, which is expressed as:

$$SINR_j^{(B)} = \frac{p_j^{(F)} g_{j,b}}{\sigma B_{UE} + \sum_{v \in \mathbb{B}_I} p_I g_{j,v}}, \tag{2.8}$$

where $g_{j,b}$ is the channel gain between FlyBS j and the BS, and $g_{j,v}$ is the channel gain between FlyBS j and neighboring BS v.

Then, as the same spectral resources are used for the whole relay link, the access is interfered by the backhaul, and thus, the access SINR is defined as:

$$SINR_{i,j}^{(A)} = \frac{p_i g_{i,j}}{\sigma B_{UE} + p_j^{(F)} g_{i,b} + \sum_{v \in \mathbb{B}_I} p_I g_{i,v}}, \tag{2.9}$$

where $p_j^{(F)}$ is the power allocated for FlyBS j at the BS, and $g_{i,b}$ is the channel gain between UE i and the BS.

Then, to obtain SINRs of individual links on a multihop path, an alternative notation is utilized. Let's consider a general object o that is part of the multihop relay, and on which the SINR is to be evaluated. Then, a sequence of FlyBSs interconnecting the object o with the BS is defined as $\mathcal{F}_o^{(M)} = \{f^{(t)}\}_{t=1}^{M_o}$, where M_o is the number of such FlyBSs. The index t does not stand for a particular FlyBS object from $\mathcal{F}$, but denotes an order in which the communication is forwarded from o to the BS via elements of $\mathcal{F}_o^{(M)}$. If the set $\mathcal{F}_o^{(M)}$ is empty, then the object o is directly associated with the BS and the SINR is evaluated according to (2.7) or (2.8) based on whether o is a UE or a FlyBS. Otherwise, the SINR of the link between object o and the FlyBS $f^{(1)}$ is given as:

$$SINR_o^{(M)} = \frac{p_{o,1} g_{o,1}}{\sigma B_{UE} + p_{M_o,b} g_{o,b} + \sum_{t \in \{1,\dots,M_o-1\}} p_{t,t+1} g_{o,t+1} + \sum_{v \in \mathcal{B}_I} p_I g_{o,v}}, \tag{2.10}$$

where $g_{o,b}$ is the gain of the channel between object o and the BS, $g_{o,1}$ is the channel gain between o and FlyBS $f^{(1)}$, and $g_{o,t+1}$ is the channel gain between o and FlyBS $f^{(t+1)}$. Then, the parameter $p_{o,1}$ stands for transmission power allocated for object o at FlyBS $f^{(1)}$, and similarly, parameters $p_{t,t+1}$ and $p_{M_o,b}$ are powers allocated to FlyBS $f^{(t)}$ by $f^{(t+1)}$ and to $f^{(M_o)}$ by the BS, respectively.

Finally, an example of all the established interference types is illustrated in Figure 2.2.

2.1.7 Channel capacity

Throughput of the communication link between two system objects is given by the Shannon capacity theorem. Therefore, the channel capacities for direct, access and backhaul links are determined as follows:

$$C_i^{(D)} = B_{UE} \log_2 \left(1 + SINR_i^{(D)}\right), \tag{2.11}$$

$$C_{i,j}^{(A)} = B_{UE} \log_2 \left(1 + SINR_{i,j}^{(A)}\right), \tag{2.12}$$

$$C_j^{(B)} = B_{UE} \log_2 \left(1 + SINR_j^{(B)}\right), \tag{2.13}$$

where specifiers (D), (A), and (B) stand for terms *direct*, *access*, and *backhaul*, respectively.

Since the capacities of the relay link $C_{i,j}^{(A)}$ and $C_j^{(B)}$ generally are not the same, the minimal of those two serves as a bottleneck for the whole UE to BS communication [20]. Therefore, the total channel capacity of the relay link is given as:

$$C_{i,j}^{(R)} = min\left(C_{i,j}^{(A)}, C_j^{(B)}\right), \tag{2.14}$$

Consequently, the final capacity experienced by UE i, based on association $\boldsymbol{A}$, power allocation $\boldsymbol{P}$ and FlyBS positions $\boldsymbol{R}$, is defined as:

$$C_i = \begin{cases} C_i^{(D)}, & a_{i,b} = 1, \\ C_{i,j}^{(R)}, & a_{i,j} = 1, \end{cases} \tag{2.15}$$

Then, to obtain an overall capacity of the multihop relay link $C_i^{(M)}$, a similar approach as in (2.12)-(2.14) is utilized. Based on the system association set $\boldsymbol{A}$, let's define a sequence of FlyBSs interconnecting the UE i with the BS as $\mathcal{F}_i^{(M)} = \{f^{(q)}\}_{q=1}^{M_i}$, where M_i is the number of FlyBSs in the multihop path to UE i. The index q does not denote a particular FlyBS object from $\mathcal{F}$, but an order in which the communication is forwarded from UE i to the BS via elements of $\mathcal{F}_i^{(M)}$. Then, let's define a set of capacities of individual links on the multihop path as $\mathbb{C}_i^{(M)} = \{C_{i,1}^{(M)}, C_{1,2}^{(M)}, ..., C_{q,q+1}^{(M)}, ..., C_{M_i,b}^{(M)}\}$, where $C_{i,1}^{(M)}$ is the capacity of the link between UE i and the first FlyBS in the path $f^{(1)}$, $C_{q,q+1}^{(M)}$ is the capacity between two consecutive FlyBSs $f^{(q)}$ and $f^{(q+1)}$, and finally, $C_{M_i,b}^{(M)}$ is the capacity

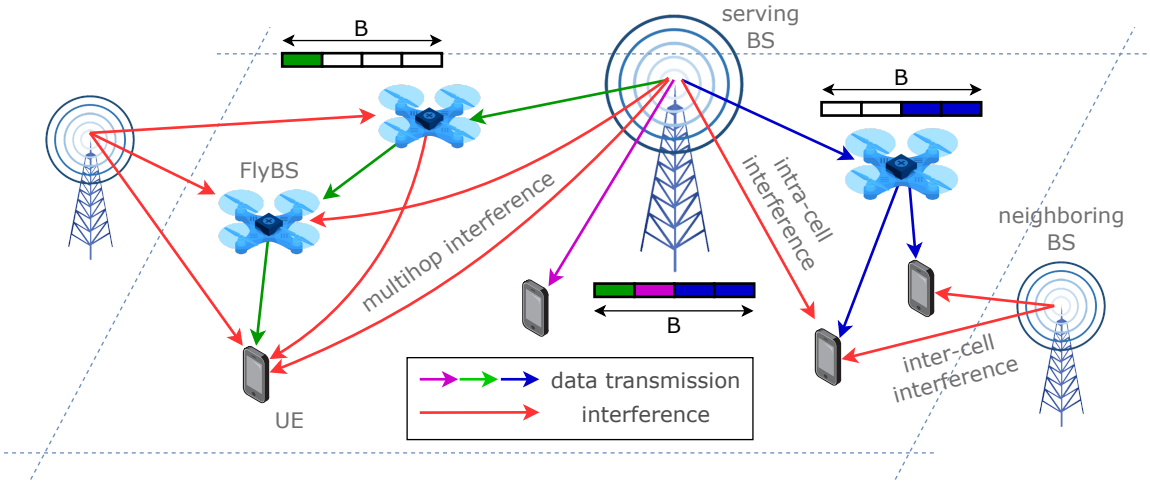

Figure 2.2: Illustrative example of interference

between the last FlyBS in $\mathcal{F}_i^{(M)}$ and the BS. As the last link to the BS is not affected by intra-cell interference at all, the capacity $C_{M_i,b}^{(M)}$ is equal to $C_j^{(B)}$, where j is the index of FlyBS $f^{(M_i)}$ in $\mathcal{F}$, and thus defined as backhaul capacity (2.13). The rest of the capacities $C_{i,1}^{(M)}$ and $C_{q,q+1}^{(M)}$ are expressed as:

$$\begin{aligned} C_{i,1}^{(M)} &= B_{UE} \log_2 \left(1 + SINR_i^{(M)}\right), \\ C_{q,q+1}^{(M)} &= B_{UE} \log_2 \left(1 + SINR_q^{(M)}\right), \end{aligned} \tag{2.16}$$

where $SINR_i^{(M)}$ is the SINR at the downlink interface of UE i, that is the SINR of the channel between UE i and the FlyBS $f^{(1)}$, and $SINR_q^{(M)}$ is the SINR of the downlink channel between FlyBSs $f^{(q)}$ and $f^{(q+1)}$. Finally, the overall capacity of the multihop relay experienced by UE i is given as:

$$C_i^{(M)} = \min\{C_{i,1}^{(M)}, C_{1,2}^{(M)}, ..., C_{q,q+1}^{(M)}, ..., C_{M_i,b}^{(M)}\}, \tag{2.17}$$

2.2 Problem formulation

The objective of this work is to maximize the minimal channel capacity among all UEs via adjusting the dynamic parameters of the system, where only direct and simple relay links via a single FlyBS are considered. In other words, the objective is to find an optimal combination of UE associations $\boldsymbol{A}^*$, transmission power allocation $\boldsymbol{P}^*$, and FlyBS positions $\boldsymbol{R}^*$, that maximizes the minimal capacity in the system. Considering this, the problem is formulated as:

$$\begin{aligned} & \boldsymbol{A}^*, \boldsymbol{P}^*, \boldsymbol{R}^* = \underset{\boldsymbol{A},\boldsymbol{P},\boldsymbol{R}}{\operatorname{argmax}} \left(\min \{C_i\}_{i=1}^{N_{UE}}\right) \\ s.t. \quad & (2.18a) \quad \sum_{i \in \mathbb{U}_j^{(F)}} p_i \leq P_F, \quad \forall j \in \mathbb{F}, \\ & (2.18b) \quad \sum_{i \in \mathbb{U}_B} p_i + \sum_{j \in \mathbb{F}} N_{UE}^{(j)} p_j^{(F)} \leq P_B, \\ & (2.18c) \quad ||\boldsymbol{a_i}||, ||\boldsymbol{a_j^{(F)}}|| = 1, \quad \forall j \in \mathbb{F}, \\ & (2.18d) \quad a_{j,b}^{(F)} = 1, \quad \forall j \in \mathbb{F}, \\ & (2.18e) \quad \{0,0\} \leq r_{flybs,j} \leq \{x_c, y_c\}, \quad \forall j \in \mathbb{F}. \end{aligned} \tag{2.18}$$

where $N_{UE}^{(j)}$ is the number of UEs associated with FlyBS j and the constraints (2.18a) and (2.18b) guarantee that the total power allocated at the BS and each of the FlyBSs, respectively, does not exceed the total transmission power available at that particular object. Then, constraint (2.18c) guarantees that each UE and FlyBS is associated only

with a single serving station. Furthermore, constraint (2.18d) restricts all FlyBSs to be associated directly with the BS only, while constraint (2.18e) limits each of the FlyBSs to be positioned only within the area of the reference cell. Note that the capacity C_i defined as (2.15) is a function of association $\boldsymbol{A}$, power allocation $\boldsymbol{P}$, and FlyBS positions $\boldsymbol{R}$.

Chapter 3

Solution proposal

In this chapter, a solution to the problem formulated in Section 2.2 is described. As solving the problem (2.18) jointly is not an easy task, it is split into three simplified subproblems, which are solved separately. To this end, first, the power allocation is found based on a general constant state of FlyBS positions and UE associations. Then, the analytical solution is utilized to solve the FlyBS positioning and association subproblems via a set of proposed heuristic algorithms. Both arguments, association and FlyBS positions, are found considering the other one static. Finally, at the end of the chapter, a joint solution to the problem (2.18) is found utilizing all of the proposed subproblem solutions.

3.1 Power allocation

In this section, the proposed power allocation that maximizes the minimal capacity is described. First, the simplified allocation subproblem is formulated, and then, it is solved via deriving an expression for allocation of power for each link in the system. Finally, the proposed power allocation scheme is analyzed and discussed.

3.1.1 Power allocation subproblem

The objective of the power allocation is to maximize the minimal channel capacity among all UEs at certain FlyBS positions $\boldsymbol{R}$ and UE associations $\boldsymbol{A}$. As the allocated bandwidth is constant and the same for all UEs in the cell according to Section 2.1.3, the transmission power is the only remaining dynamic parameter on which channel capacity depends. Then, the maximization of minimal capacity can be achieved via utilizing all of the available power resources in a way, that each of the UEs in the cell has the same capacity. This is supported by the fact that any further boost of any of the UE's capacity would only compromise the other UEs and decrease the minimum, as no other power resources would

be available. Hence, without a loss of generality, the desired maximization of minimal capacity can be translated to the maximization of equalized common capacity.

Then, the problem (2.18) is simplified and reformulated as:

$$\begin{aligned} & \boldsymbol{P^*} = \underset{\boldsymbol{P}}{\operatorname{argmax}} \left(C_i\right) \\ s.t. \quad & (3.1a) \qquad C_i = C, \quad \forall i \in \mathbb{U}, \\ & (3.1b) \qquad \sum_{i \in \mathbb{U}_j^{(F)}} p_i \leq P_F, \quad \forall j \in \mathbb{F}, \\ & (3.1c) \qquad \sum_{i \in \mathbb{U}_B} p_i + \sum_{j \in \mathbb{F}} N_{UE}^{(j)} p_j^{(F)} \leq P_B, \end{aligned} \tag{3.1}$$

where C_i is the end-to-end channel capacity experienced by UE i according to (2.15) and is equal to common capacity C, which is the same for all UEs in the cell, as specified by constraint (3.1a). Then, the constraints (3.1b) and (3.1c) are the same as in (2.18) and guarantee that the allocated power does not exceed the total power available.

As the desired channel capacity should be of the same value for every UE in the cell, the maximization of minimal capacity is implied by the maximization of sole value C. Furthermore, to maximize the end-to-end capacity of the relay link, capacities of both access and backhaul links should be the same according to (2.14), otherwise one of them would serve as a bottleneck. Thus, the common capacity C is in (3.1) substituted by partial capacity c common for every single link in the cell, that is each direct, access, and backhaul link. Note that the bandwidth allocated for each channel in the cell is the same according to Section 2.1.3. Then, considering channel capacity evaluation according to (2.11)-(2.13), the partial capacity is purely proportional to the SINR of the link and as such can be replaced by it in the problem formulation. Hence, the optimization problem (3.1) is further simplified and rewritten as:

$$\begin{aligned} & \boldsymbol{P^*} = \underset{\boldsymbol{P}}{\operatorname{argmax}}(s) \\ s.t. \quad & (3.2a) \qquad s = s_i = s_j, \quad \forall i \in \mathbb{U}, \quad \forall j \in \mathbb{F} \\ & (3.2b) \qquad \sum_{i \in \mathbb{U}_j^{(F)}} p_i \leq P_F, \quad \forall j \in \mathbb{F}, \\ & (3.2c) \qquad \sum_{i \in \mathbb{U}_B} p_i + \sum_{j \in \mathbb{F}} p_j^{(F)} \leq P_B, \end{aligned} \tag{3.2}$$

where variable s is the SINR common for each downlink channel in the cell. Then, parameter s_i denotes the SINR of the access channel between UE i and FlyBS j or the

direct link between UE i and the BS. Similarly, parameter s_j stands for the SINR of the backhaul link between FlyBS j and the BS.

To find a solution to the problem (3.2), first, a scenario with only a single serving station (e.g. the BS with no FlyBS support) is examined. Then, the problem is solved for a single UE associated with a single FlyBS in the cell, after which the solution is generalized for an arbitrary set of UEs and FlyBSs.

3.1.2 Single serving station

Let's consider a radio access system with only a single serving station, which all UEs in the cell are associated with. All communication channels are interfered only by surrounding cells, whose configuration is not relevant, as the interference value of a communication link is considered to be acquired prior to the evaluation, and as such is a constant for the instantaneous power allocation. Then, given the general SINR expressed according to (2.7), the SINR of the communication link between UE i and the BS is simplified to:

$$s_i = \frac{p_i g_{i,b}}{n + i_i}, \quad \forall i \in \mathbb{U}, \tag{3.3}$$

where $i_i = \sum_{v \in \mathbb{B}_I} p_I g_{i,v}$ is the inter-cell interference, n is the noise common for all UEs in the cell, p_i is the transmission power allocated for UE i, and $g_{i,b}$ is the gain of the channel between UE i and the BS. The established model is illustrated in Figure 3.1. Note that the model can be applied to any arbitrary serving station, which is not affected by interference from within the cell.

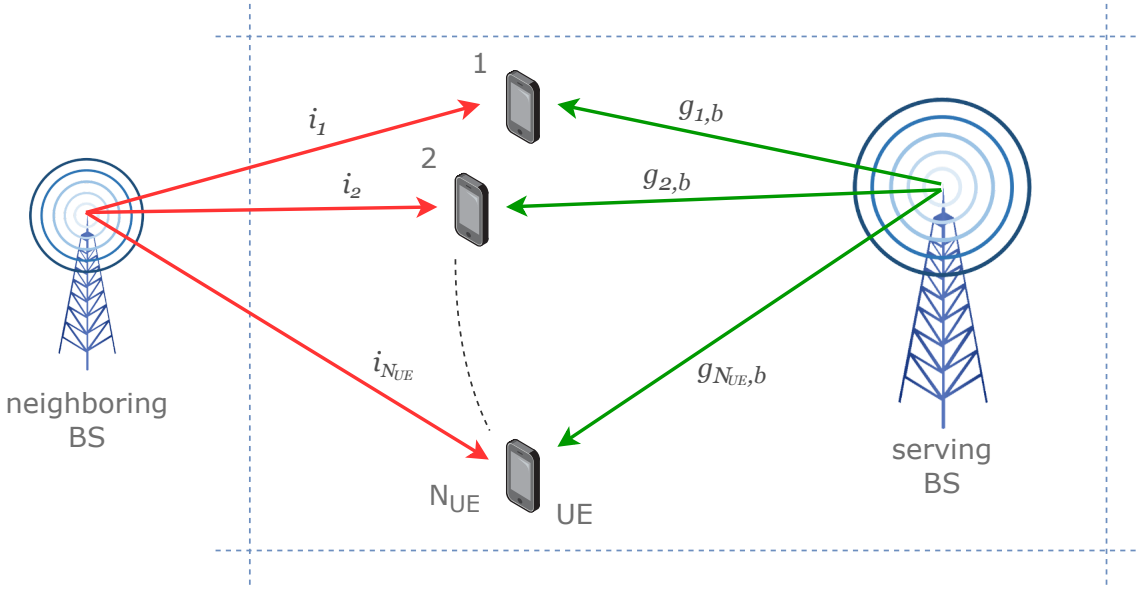

Figure 3.1: System model for power allocation at a single serving station

Having the model established, let's focus on the power allocation now. To ensure maximization of the SINR s, and thus, maximization of the common capacity C, the whole power budget of the BS P_B should be utilized. Then, the following equation applies:

$$P_B = p_1 + p_2 + ... + p_{N_{UE}} = \sum_{i=1}^{N_{UE}} p_i. \tag{3.4}$$

Then, according to (3.3), the allocated transmission power p_i is further expressed as:

$$p_i = \frac{s_i \left(n + i_i\right)}{g_{i,b}}, \tag{3.5}$$

and thus, the equation (3.4) is rewritten to:

$$P_B = p_1 + p_2 + ... + p_{N_{UE}} = \sum_{i=1}^{N_{UE}} \frac{s_i \left(n + i_i\right)}{g_{i,b}}. \tag{3.6}$$

Subsequently, considering parameter s_i to be of the same value s for each UE i, after several mathematical operations, (3.6) is rewritten and the common SINR value is expressed as:

$$s = \frac{P_B}{\sum_{i=1}^{N_{UE}} \frac{\left(n + i_i\right)}{g_{i,b}}}. \tag{3.7}$$

Finally, by substituting s_i in (3.5) with (3.7), the final power allocation that ensures the end-to-end capacity equalization is concluded in the following lemma.

Lemma 1. *The optimal transmission power allocated to UE i at the BS not affected by intra-cell interference, which ensures equalized channel capacity for all UEs, that is $C_i = C \ \forall i \in \mathbb{U}_B$, is:*

$$p_i = \frac{\left(n + i_i\right)}{g_{i,b}} \frac{P_B}{\sum_{i=1}^{N_{UE}} \frac{\left(n + i_i\right)}{g_{i,b}}}. \tag{3.8}$$

Proof. Accordning to Lemma 1, the power received by the UE i is expressed as:

$$p_i^{(r)} = p_i g_{i,b} = \frac{\left(n + i_i\right)}{g_{i,b}} \frac{g_{i,b} P_B}{\sum_{i=1}^{N_{UE}} \frac{\left(n + i_i\right)}{g_{i,b}}} = \frac{\left(n + i_i\right) P_B}{\sum_{i=1}^{N_{UE}} \frac{\left(n + i_i\right)}{g_{i,b}}}, \tag{3.9}$$

where the $(n + i_i)$ in numerator of the form is the only variable term depending on i, the

rest is a constant. Now, let's define channel capacity experienced by the UE i as:

$$C_i = B \log_2 \left(1 + \frac{p_i^{(r)}}{n + i_i} \right). \tag{3.10}$$

Then, substituting $p_i^{(r)}$ in (3.10) with (3.9) results in canceling the variable term $(n + i_i)$, such that:

$$C_i = B \log_2 \left(1 + \frac{P_B}{\sum_{i=1}^{N_{UE}} \frac{(n + i_i)}{g_{i,b}}} \right), \tag{3.11}$$

where the resulting argument of the logarithm is a constant. Thus, all capacities are equal regardless of the value i, or in other words, $C_i = C \ \forall i \in \mathbb{U}_B$, that is every UE in the cell. This concludes the proof. □

3.1.3 Capacity equalization of a single relay link

By introducing a relay link where the same bandwidth resources are used for both access and backhaul, the capacity equalization on those two links generally gets more complicated compared to the simple scenario described in Section 3.1.2. Specifically, the following two problems need to be addressed:

i) The access link is interfered by the backhaul, which results in the access interference no longer being a constant for each UE individually. Furthermore, its variable intra-cell part is dependent on the transmission power allocated for backhaul at the BS. Therefore, the two transmission powers, access and backhaul, need to be allocated simultaneously.

ii) A second restriction for total allocated power is introduced. Transmission powers for access and backhaul are both allocated on different serving stations, that is FlyBS and BS, respectively, with different and mutually independent power budgets.

With the new problems introduced, let's consider a simple scenario, where the only UE in the cell is associated with the only FlyBS in the cell. The backhaul communication between the BS and the FlyBS serves as interference to the UE. The described scenario model is illustrated in Figure 3.2.

To equalize the capacities of both backhaul and access and ensure none of them would be a bottleneck, a common SINR value s is required for both of the links. Then, according to the SINR formula (2.8), the power allocated at backhaul should be:

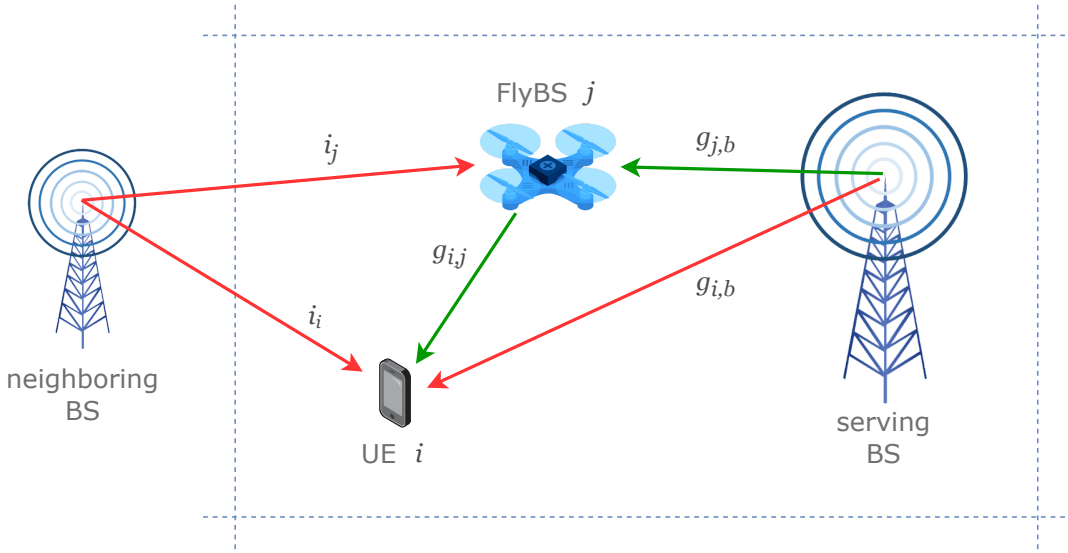

Figure 3.2: System model for a single relay link power allocation

$$p_j = \frac{s\,(n + i_j)}{g_{j,b}} \leq P_B, \tag{3.12}$$

where n is the noise and index j denotes the only FlyBS in the cell. Thus, the parameter $g_{j,b}$ is the channel gain between FlyBS j and the BS, P_B is the total power available for downlink communication at the BS and i_j is the interference from surrounding cells to the FlyBS's backhaul, that is $i_j = \sum_{v \in \mathbb{B}_I} p_I g_{j,v},$. Then, considering the interference from backhaul and (2.9), the following equation should apply for the power allocated at access:

$$p_i = \frac{s\,(n + i_i + p_j g_{i,b})}{g_{i,j}} \leq P_F, \tag{3.13}$$

where index i denotes the only UE in the cell, and thus, $g_{i,j}$ is the gain of the access channel between UE i and FlyBS j, i_i is the interference from surrounding cells to the access link, that is $i_i = \sum_{v \in \mathbb{B}_I} p_I g_{i,v}$, and P_F is the total power available for downlink communication at the FlyBS. Then, parameter $g_{i,b}$ is the gain of the direct propagation path between the BS and the UE, and thus the term $p_j g_{i,b}$ stands for interference from the backhaul to the access.

Then, in order to satisfy both power restriction conditions (3.2b) and (3.2c), the two inequalities (3.12) and (3.13), where s is the unknown variable, should be solved jointly. This requires first solving each of them separately and acquiring solution intervals $\mathcal{S}_B$ and $\mathcal{S}_F$ for power allocated at the BS (3.12) and power allocated at the FlyBS (3.13), respectively. The joint solution is then found as $\max(\mathcal{S}_B \cap \mathcal{S}_F)$, which maximizes the common SINR value of both access and backhaul links, and thus maximizes the end-to-end channel capacity. The final power allocation for access and backhaul is defined in Lemma 2.

Lemma 2. *Considering a single relay link UE-FlyBS-BS, the optimal transmission powers allocated for backhaul at the BS p_j and access at the FlyBS p_i, that ensure equalized and maximized channel capacities for both of these links, are:*

$$\begin{aligned} p_j &= \frac{s\left(n+i_j\right)}{g_{j,b}}, \\ p_i &= \frac{s\left(n+i_i+p_j g_{i,b}\right)}{g_{i,j}}, \end{aligned} \tag{3.14}$$

where:

$$s = \min\left\{ \frac{P_B g_{j,b}}{n+i_j}; \frac{\sqrt{\left(n+i_i\right)^2 + 4P_F \frac{g_{i,j}g_{i,b}}{g_{j,b}}\left(n+i_j\right)} - \left(n+i_i\right)}{2\left(n+i_j\right)\frac{g_{i,b}}{g_{j,b}}} \right\}. \tag{3.15}$$

Proof. As has been stated, the inequalities (3.12) and (3.13) should be solved separately first. Let's focus on the backhaul power allocation. After several mathematical operations, the form (3.12) is rewritten as:

$$s \leq \frac{P_B g_{j,b}}{n+i_j}. \tag{3.16}$$

Then, the solution to this inequality is given by interval $\mathcal{S}_B = \left(0; s^{(B)}\right\rangle = \left\langle 0; \frac{P_B g_{j,b}}{n+i_j}\right\rangle$, where $s \in \mathcal{S}_B$, as the SINR cannot be in definition lower than or equal to zero according to (2.8). To solve the access power inequality (3.13), first, the parameter p_j is substituted with its definition in (3.12), so that:

$$\frac{s\left(n+i_i+s\frac{n+i_j}{g_{j,b}}g_{i,b}\right)}{g_{i,j}} \leq P_F. \tag{3.17}$$

After several mathematical operations, the newly obtained inequality (3.17) is rewritten to:

$$s^2\left(\left(n+i_j\right)\frac{g_{i,b}}{g_{j,b}}\right) + s\left(n+i_i\right) - P_F g_{i,j} \leq 0, \tag{3.18}$$

which is a quadratic inequality to be solved by the use of quadratic formula. Discriminant of the formula is given as:

$$D = \left(n+i_i\right)^2 + 4P_F g_{i,j}\frac{g_{i,b}}{g_{j,b}}\left(n+i_j\right). \tag{3.19}$$

As all of the parameters in (3.19) are real positive numbers, the discriminant D is also a real positive number, and thus the quadratic inequality (3.18) has a real solution. Then,

the two real roots of (3.18) are given as:

$$\begin{aligned} s_1 &= \frac{-\left(n+i_i\right) + \sqrt{\left(n+i_i\right)^2 + 4P_F \frac{g_{i,j}g_{i,b}}{g_{j,b}}\left(n+i_j\right)}}{2\left(n+i_j\right)\frac{g_{i,b}}{g_{j,b}}}, \\ s_2 &= \frac{-\left(n+i_i\right) - \sqrt{\left(n+i_i\right)^2 + 4P_F \frac{g_{i,j}g_{i,b}}{g_{j,b}}\left(n+i_j\right)}}{2\left(n+i_j\right)\frac{g_{i,b}}{g_{j,b}}}, \end{aligned} \tag{3.20}$$

where only s_1 is a positive number as:

$$\sqrt{\left(n+i_i\right)^2 + 4P_F \frac{g_{i,j}g_{i,b}}{g_{j,b}}\left(n+i_j\right)} > \left(n+i_i\right), \tag{3.21}$$

because:

$$\begin{gathered} \left(n+i_i\right)^2 + 4P_F \frac{g_{i,j}g_{i,b}}{g_{j,b}}\left(n+i_j\right) > \left(n+i_i\right)^2, \\ 4P_F \frac{g_{i,j}g_{i,b}}{g_{j,b}}\left(n+i_j\right) > 0. \end{gathered} \tag{3.22}$$

Then, the resulting SINR that satisfies the inequality (3.18) lies in the interval $\mathcal{S}_A = \left(0; s^{(A)}\right\rangle = (0; s_1\rangle$. Finally, the joint solution of (3.12) and (3.13) is given by the intersection of intervals $\mathcal{S}_B$ and $\mathcal{S}_A$. To maximize the SINR, and thus the common channel capacity, the maximum of the intersection is taken as $s = \max\left(\mathcal{S}_A \cap \mathcal{S}_B\right) = \min\{s^{(A)}, s^{(B)}\}$. Considering the transmission power formulas for access and backhaul from (3.13) and (3.12), respectively, this directly leads to forms (3.14) and (3.15) defined in Lemma 2, and thus concludes the proof. □

3.1.4 General problem solution

In order to solve the power allocation problem (3.2) for a general FlyBS-supported radio access system, the two previously examined simplified scenarios are combined and their solutions generalized. To this end, first, a general scenario model is established as illustrated in Figure 3.3. The system is identical to the model described in Section 2.1. That is, the BS is supported by N_{FlyBS} FlyBSs, where each FlyBS j serves $N_{UE}^{(j)}$ UEs, while the rest of $N_{UE}^{(b)}$ UEs are associated directly with the BS. As in Sections 3.1.2 and 3.1.3, the channels in the system are described by channel gain and inter-cell interference, which are both constant for the instantaneous power allocation and each object individually.

With the model specified, let's focus on the power allocation constraints. According to problem constraints (3.2b) and (3.2c), the total power allocated for downlink communication in the cell must satisfy the following system of conditions:

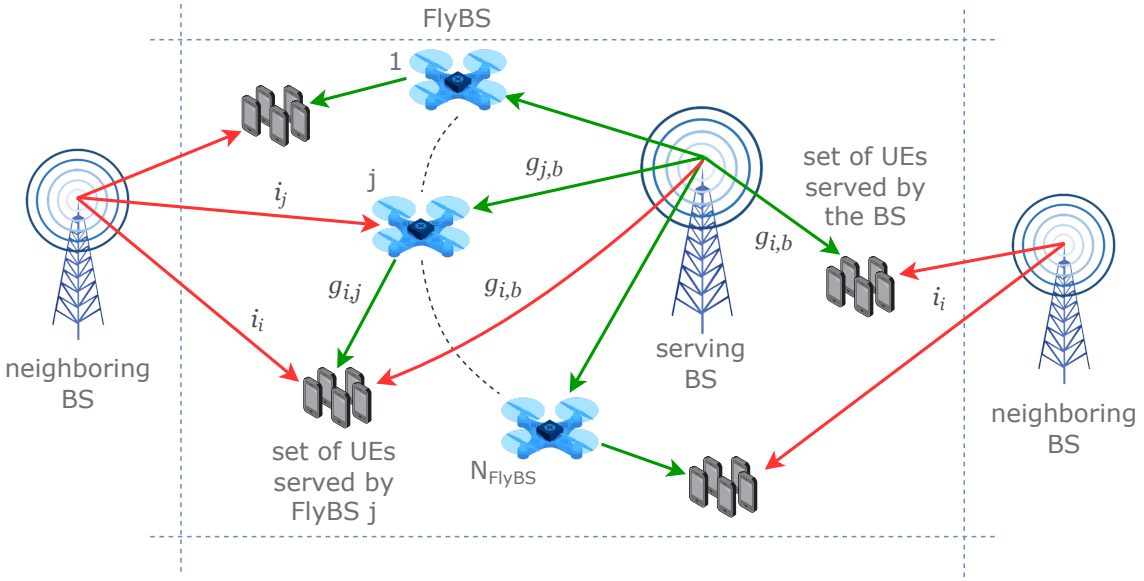

Figure 3.3: System model for power allocation in a general FlyBS-supported cell

$$\sum_{i \in \mathbb{U}_B} p_i + \sum_{j \in \mathbb{F}} N_{UE}^{(j)} p_j^{(F)} \leq P_B, \tag{3.23}$$

$$\sum_{i \in \mathbb{U}_j^{(F)}} p_i \leq P_F, \tag{3.24}$$

where parameter p_i is the transmission power allocated either for the direct channel between UE i and the BS, or the access channel between UE i and the FlyBS j, while $p_j^{(F)}$ is the power allocated for the backhaul link between the BS and the FlyBS j. Transmission powers p_i and $p_j^{(F)}$ are, with respect to the desired common SINR and according to (2.7)–(2.9), expressed as:

$$p_j^{(F)} = \frac{s\,(n + i_j)}{g_{j,b}}, \tag{3.25a}$$

$$p_i = \begin{cases} \dfrac{s\,(n + i_i)}{g_{i,b}}, & \text{if } a_{i,b} = 1, \\ \dfrac{s\left(n + i_i + p_j^{(F)} g_{i,b}\right)}{g_{i,j}}, & \text{if } a_{i,j} = 1, \end{cases} \tag{3.25b}$$

where i_i and i_j are the interferences from surrounding cells to UE i and FlyBS j, respectively.

Analogous to Section 3.1.3, to equalize and maximize the channel capacity in the system, the resulting common SINR s must satisfy both inequalities (3.23) and (3.24). To this end, the transmission powers are substituted with their definitions (3.25) and the power allocation restrictions (3.23) and (3.24) are rewritten to:

$$\sum_{i\in\mathbb{U}_B} \frac{s}{g_{i,b}}\left(n+i_i\right) + \sum_{j\in\mathbb{F}} N_{UE}^{(j)} \frac{s}{g_{j,b}}\left(n+i_j\right) \leq P_B, \tag{3.26a}$$

$$\sum_{i\in\mathbb{U}_j^{(F)}} \frac{s}{g_{i,j}}\left(n+i_i+p_j^{(F)}g_{i,b}\right) \leq P_F, \quad \forall j \in \{1,...,N_{FlyBS}\}. \tag{3.26b}$$

The system of inequalities is then solved by utilizing a similar approach as for a single UE-FlyBS-BS relay link described in Section 3.1.3. Finally, by finding the maximum SINR in the acquired set of solutions, one arrives at the final general power allocation defined in the following Lemma.

Lemma 3. *The optimal transmission powers p_i and $p_j^{(F)}$ allocated for downlink communication to UE i and FlyBS j, respectively, that ensure equalized and maximized end-to-end capacities among all UEs in the cell, are defined as:*

$$p_j^{(F)} = \frac{s\left(n+i_j\right)}{g_{j,b}},$$

$$p_i = \begin{cases} \dfrac{s\left(n+i_i\right)}{g_{i,b}}, & \text{if UE } i \text{ is associated with the BS,} \\ \dfrac{s\left(n+i_i+p_j^{(F)}g_{i,b}\right)}{g_{i,j}}, & \text{if UE } i \text{ is associated with the FlyBS } j. \end{cases} \tag{3.27}$$

The parameter s is the SINR common for all links in the system and is defined as:

$$s = \min\left\{s^{(B)}, s_1^{(F)}, ..., s_j^{(F)}, s_{j+1}^{(F)}, ..., s_{N_{FlyBS}}^{(F)}\right\}, \tag{3.28}$$

where:

$$s^{(B)} = \frac{P_B}{\sum\limits_{i\in\mathbb{U}_B} \frac{1}{g_{i,b}}\left(n+i_i\right) + \sum\limits_{j\in\mathbb{U}_j^{(F)}} \frac{N_{UE}^{(j)}}{g_{j,b}}\left(n+i_j\right)}, \tag{3.29a}$$

$$s_j^{(F)} = \frac{\sqrt{B_j^2+4A_jC_j}-B_j}{2A_j}, \quad \forall j \in \{1,...,N_{FlyBS}\}, \tag{3.29b}$$

and:

$$A_j = \frac{(n+i_j)}{g_{j,b}} \left[\sum_{i \in \mathbb{U}_j^{(F)}} \left(g_{i,b} \prod_{i' \in \mathbb{U}_j^{(F)} \setminus \{i\}} g_{i',j} \right) \right], \tag{3.30a}$$

$$B_j = \sum_{i \in \mathbb{U}_j^{(F)}} \left((n+i_i) \prod_{i' \in \mathbb{U}_j^{(F)} \setminus \{i\}} g_{i',j} \right), \tag{3.30b}$$

$$C_j = P_F \prod_{i \in \mathbb{U}_j^{(F)}} g_{i,j}. \tag{3.30c}$$

Proof. To find a solution to the system of inequalities (3.26), each inequality should be solved separately, after which the joint solution is given as an intersection of partial solutions. To this end, given the characteristics of (3.26), solving only two inequalities is sufficient: the one defining the BS restriction (3.26a) and the one defining the power restriction of a general FlyBS (3.26b). First, let's focus on the BS inequality. After a few mathematical operations, the form (3.26a) is rewritten to:

$$s \leq \frac{P_B}{\sum\limits_{i \in \mathbb{U}_B} \frac{1}{g_{i,b}} (n+i_i) + \sum\limits_{j \in \mathbb{U}_j^{(F)}} N_{UE}^{(j)} \frac{1}{g_{j,b}} (n+i_j)} = s^{(B)}. \tag{3.31}$$

Then, the set of solutions is given by the interval $\mathcal{S}_B = \left(0; s^{(B)}\right\rangle$, where $s \in \mathcal{S}_B$. The interval is bounded below by zero, as the SINR cannot be lower than or equal to zero according to definitions (2.7)–(2.9). For the general FlyBS power restriction inequality, first, both sides of the form (3.26b) are multiplied by the product of all channel gains between UEs i and their associated FlyBSs j, as follows:

$$\sum_{i \in \mathbb{U}_j^{(F)}} \left[s \left(n + i_i + p_j^{(F)} g_{i,b} \right) \prod_{i' \in \mathbb{U}_j^{(F)} \setminus \{i\}} g_{i',j} \right] \leq P_F \prod_{i \in \mathbb{U}_j^{(F)}} g_{i,j}, \quad \forall j \in \{1, ..., N_{FlyBS}\}. \tag{3.32}$$

Consequently, substituting the power allocated at the backhaul $p_j^{(F)}$ with (3.25a) and performing several other mathematical operations, the inequality (3.32) is further rewritten to:

$$\sum_{i \in \mathbb{U}_j^{(F)}} \left[\left(s (n+i_i) + s^2 (n+i_j) \frac{g_{i,b}}{g_{j,b}} \right) \prod_{i' \in \mathbb{U}_j^{(F)} \setminus \{i\}} g_{i',j} \right] - P_F \prod_{i \in \mathbb{U}_j^{(F)}} g_{i,j} \leq 0, \tag{3.33}$$
$$\forall j \in \{1, ..., N_{FlyBS}\}.$$

Then, the sum is split into two, expressing the form (3.33) as a quadratic inequality:

$$\frac{s^2}{g_{j,b}}(n+i_j)\sum_{i\in\mathbb{U}_j^{(F)}}\left[g_{i,b}\prod_{i'\in\mathbb{U}_j^{(F)}\setminus\{i\}}g_{i',j}\right]+s\sum_{i\in\mathbb{U}_j^{(F)}}\left[(n+i_i)\prod_{i'\in\mathbb{U}_j^{(F)}\setminus\{i\}}g_{i',j}\right]- \\ -P_F\prod_{i\in\mathbb{U}_j^{(F)}}g_{i,j}\leq 0,\quad \forall j\in\{1,...,N_{FlyBS}\}, \tag{3.34}$$

which is for further examination simplified as:

$$s^2A_j+sB_j-C_j\leq 0,\quad \forall j\in\{1,...,N_{FlyBS}\}, \tag{3.35}$$

where:

$$A_j=\frac{(n+i_j)}{g_{j,b}}\sum_{i\in\mathbb{U}_j^{(F)}}\left[g_{i,b}\prod_{i'\in\mathbb{U}_j^{(F)}\setminus\{i\}}g_{i',j}\right], \tag{3.36a}$$

$$B_j=\sum_{i\in\mathbb{U}_j^{(F)}}\left[(n+i_i)\prod_{i'\in\mathbb{U}_j^{(F)}\setminus\{i\}}g_{i',j}\right], \tag{3.36b}$$

$$C_j=P_F\prod_{i\in\mathbb{U}_j^{(F)}}g_{i,j}. \tag{3.36c}$$

The solution to the quadratic inequality (3.35) is then found by the use of quadratic formula, where the discriminant $D=B_j^2+4A_jC_j$ is always a positive real number. Therefore, roots of the quadratic term in (3.35) are expressed as:

$$s_1=\frac{-B_j+\sqrt{B_j^2+4A_jC_j}}{2A_j}, \\ s_2=\frac{-B_j-\sqrt{B_j^2+4A_jC_j}}{2A_j}, \tag{3.37}$$

where only $s_1=s_j^{(F)}$ is positive as:

$$\sqrt{B_j^2+4A_jC_j}>B_j, \tag{3.38}$$

because:

$$B_j^2+4A_jC_j>B_j^2, \\ 4A_jC_j>0. \tag{3.39}$$

Therefore, the solution to the inequality (3.26b) is for a general FlyBS j given by the interval $\mathcal{S}_j^{(F)} = \left(0; s_j^{(F)}\right\rangle$, where $s \in \mathcal{S}_j^{(F)}$. Finally, the overall joint solution to the system of inequalities (3.26) is given by the intersection of partial solutions $\{\mathcal{S}_B, \mathcal{S}_1^{(F)}, ..., \mathcal{S}_{N_{FlyBS}}^{(F)}\}$ as $\mathcal{S} = \mathcal{S}_B \cap \mathcal{S}_1^{(F)} \cap ... \cap \mathcal{S}_{N_{FlyBS}}^{(F)}$. Then, to maximize the common SINR, and thus the equalized channel capacity, the final s is acquired as the maximum of joint solution interval $\mathcal{S}$ as:

$$s = \max(\mathcal{S}) = \max\left(\mathcal{S}_B \cap \mathcal{S}_1^{(F)} \cap ... \cap \mathcal{S}_{N_{FlyBS}}^{(F)}\right) = \min\left\{s^{(B)}, s_1^{(F)}, ..., s_{N_{FlyBS}}^{(F)}\right\}. \quad (3.40)$$

This, in addition to the transmission power definitions (3.25), directly leads to relations (3.27)-(3.30) defined in Lemma 3, and thus concludes the proof. □

3.1.5 Proposed scheme discussion

Having the general power allocation scheme described and established, let's discuss the implications of its deployment. Note that according to relations defined in Lemma 3, the power allocation is based purely on channel quality parameters, specifically the channel gain, interference, and noise, all of which are considered to be known constants for each UE at the time of evaluation. Therefore, given that interference is a function of propagation gain and noise has the same value for all objects, the proposed power allocation is suitable for any arbitrary path loss or noise model, whether it is a theoretical model or an actual measured value, as the scheme uses only the resulting values as input parameters. Moreover, the proposed power allocation can be in general utilized for both LoS and NLoS environments, given that the scheme is supplied with a real measured channel gain or a suitable path loss model. However, the scheme is designed to equalize channel capacity only within a single cell. Thus, it is not possible to equalize capacities among multiple cells via utilization of the proposed power allocation scheme as described in Lemma 3.

Furthermore, the proposed scheme has an interesting effect on the utilization of each object's total power budget. To clarify this, let's first examine the final common SINR evaluation (3.40) as described in Lemma 3. The set $\mathbb{S} = \{s^{(B)}, s_1^{(F)}, ..., s_j^{(F)}, s_{j+1}^{(F)}, ..., s_L^{(F)}\}$ is in fact a set of SINR values each serving station is able to provide for downlink channels managed by it, fully utilizing its power budget. Then, as the minimal value of $\mathbb{S}$ is assigned to all of the serving stations, only the one providing the minimal SINR is fully utilized. Thus, this station serves as a power allocation bottleneck, as it determines the final common capacity in the cell and restricts all other serving stations from utilizing more power. The bottleneck is given as:

$$\boldsymbol{b} = \underset{o \in \mathcal{O}}{\operatorname{argmin}} \left(s_o \right), \tag{3.41}$$

where $\mathcal{O}$ is a set of all serving stations, $o \in \mathcal{O}$ stands for an arbitrary station, that is either the BS or a particular FlyBS, and $s_o \in \mathbb{S}$ is defined as:

$$s_o = \begin{cases} s^{(B)}, & \text{if } o \text{ is the BS,} \\ s_j^{(F)}, & \text{if } o \text{ is the FlyBS } j. \end{cases} \tag{3.42}$$

3.2 Positioning of Flying Base Stations

In this section, a scheme for power-efficient positioning of individual FlyBSs in the cell is proposed. First, the positioning subproblem is simplified and reformulated, and then, it is solved via the implementation of a heuristic positioning algorithm.

3.2.1 Positioning subproblem

The objective of the positioning subproblem is to maximize the minimal capacity among all UEs in the cell for given UE to BS/FlyBS associations via positioning of the FlyBSs. However, as the power allocation scheme proposed in Section 3.1 is utilized, the problem translates to the maximization of the common capacity. Note that as the common capacity is given by the power allocation bottleneck, its maximization is achieved when all of the serving stations in the cell are fully utilized, e.i., no bottleneck is present in the system. Therefore, the objective of the FlyBS positioning is reformulated as maximization of the FlyBS power efficiency deployment, or in other words, maximization of individual serving stations' power utilization. Thus, the objective is given as:

$$\begin{aligned} \boldsymbol{R}^* &= \underset{\boldsymbol{R}}{\operatorname{argmax}} \left(\frac{P_B^{(util)}}{P_B} + \sum_{j \in \mathbb{F}} \frac{P_j^{(util)}}{P_F} \right), \\ s.t. \qquad (3.43a) \qquad & \{0,0\} \leq r_{flybs,j} \leq \{x_c, y_c\}, \quad \forall j \in \mathbb{F}. \end{aligned} \tag{3.43}$$

where $P_B^{(util)}$ and $P_j^{(util)}$ are the total utilized transmission powers of the BS and FlyBS j, respectively. The constraint (3.43a) is the same as in (2.18) and restricts each of the FlyBSs to be positioned only within the area of the reference cell.

As the power allocation depends on the positions of FlyBSs, considering the solution to the power allocation problem described in Section 3.1, finding an analytical solution to the positioning problem (3.43) is complex if not infeasible and thus is out of the scope of this work. However, as the FlyBS positions should be evaluated in real time, that is in the time period for which the UE positions can be considered a constant, a potential algorithm

leading to an optimal solution to the problem (3.43) also faces complexity constraints. In the context of this, the solution settles for a suboptimal result and proposes a heuristic iterative algorithm that determines the FlyBS positions in real time using a specially designed power allocation force field. In each iteration of the algorithm, a new position for each FlyBS is found based on the current state of the system, until all FlyBSs converge to their final positions. To save power and time consumed by the additional and unnecessary movement of the FlyBS, the proposed positioning algorithm is executed virtually without actual FlyBS repositioning via exploiting the channel quality prediction based on [27][28]. Then, the real FlyBS is relocated only to its final position. Virtualization of the algorithm is possible via utilization of the path loss prediction described in Section 2.1.5, by means of which the propagation gains of UE-FlyBS and FlyBS-BS links are evaluated for each intermediate virtual FlyBS position.

3.2.2 Force field establishment

The proposed positioning solution is inspired by the utilization of virtual forces described in [21], which establishes force interactions between network objects similar to electrostatic forces to determine the FlyBS initial positions. However, unlike [21], the proposed solution utilizes forces depending on the power allocation instead of distances between individual objects to better address the positioning problem (3.43). Moreover, only attraction forces are considered, as there is no need for repulsive forces when the inter-cell interference is already included in the power allocation evaluation and all of the FlyBSs use different spectral resources, i.e., do not interfere each other.

With the general interaction characteristics established, a virtual vector field that mediates mutual force interactions between objects in the cell is proposed. Given that the force system is only used for positioning the FlyBSs, defining a general force interaction between two arbitrary objects is not necessary. Therefore, only two force types, both experienced by the FlyBS, are specified: a *backhaul force*, where the source is the BS, and an *access force*, where the source is the UE. Both of these forces are designed to mediate the FlyBS positions to relieve the more loaded serving objects, and to this end, reflect the current power utilization relations in the cell. The *backhaul force* applied by the BS to the FlyBS j is given as:

$$\vec{F}_{j,b}^{(B)} = \frac{P_B^{(util)}}{P_B} \frac{r_{bs} - r_{flybs,j}}{||r_{bs} - r_{flybs,j}||}, \tag{3.44}$$

where $P_B^{(util)}$ is the total power utilized by the BS, P_B is the total power budget of the BS, while r_{bs} and $r_{flybs,j}$ are the $\mathbb{R}^2$ positions of the BS and FlyBS j, respectively. That is, z coordinates of both positions are considered zero. Then, the operator $||.||$ denotes the

evaluation of Euclidean distance. The *access force* applied to the FlyBS j by associated UE i is then expressed as:

$$\vec{F}_{i,j}^{(A)} = \frac{p_i}{P_F} \frac{r_{ue,i} - r_{flybs,j}}{||r_{ue,i} - r_{flybs,j}||}, \tag{3.45}$$

where p_i is the transmission power allocated to UE i at FlyBS j, P_F is the total power budget of the FlyBS for downlink communication and $r_{ue,i}$ is an $\mathbb{R}^2$ position of the UE.

Finally, having all of the individual system forces necessary for FlyBS positioning specified, the overall net force applied to the FlyBS j is evaluated as:

$$\vec{F}_j = \vec{F}_{j,b}^{(B)} + \sum_{i \in \mathbb{U}_j^{(F)}} \vec{F}_{i,j}^{(A)}, \tag{3.46}$$

where $\mathbb{U}_j^{(F)}$ is the set of indices of UEs associated with the FlyBS j. The established positioning forces applied to the FlyBS are illustrated in Figure 3.4.

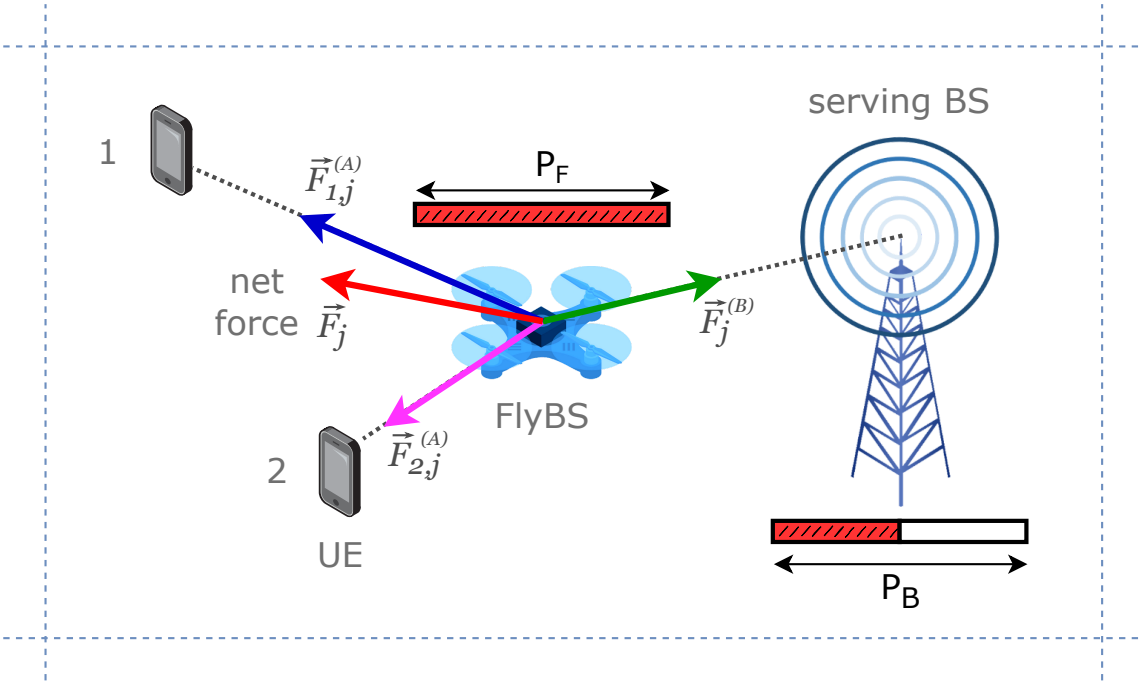

Figure 3.4: Illustrative example of positioning forces

Then, with both access and backhaul forces being the forces of attraction, the affected FlyBS is continuously shifted in a direction of the net force, with an intensity proportional to its magnitude, as in a conventional physical force field. The shift continues until a point of mechanical equilibrium is reached, that is a point where the sum of forces acting on the FlyBS is close to zero, i.e., the net force magnitude is lower than or equal to toleration specified by value ϵ.

3.2.3 Positioning of FlyBSs via the system of forces

As the forces defined in Section 3.2.2 are purely based on power allocation variables, they depend on the FlyBS positions and thus change with any FlyBS position shift in the cell. Therefore, it is necessary to divide the positioning of a single FlyBS into separate steps, where each consists of a FlyBS position shift by a given distance and subsequent reallocation of the power in the cell. Furthermore, note that as changing the position of one arbitrary FlyBS affects power allocation in the whole cell, the FlyBSs cannot be positioned one by one. That is, relocating only the FlyBS j at a time completely changes the power allocation which the evaluation of (j–1)-th FlyBS position has been based on. Thus, the FlyBSs have to be positioned simultaneously.

Considering this, the proposed solution implements a heuristic algorithm inspired by [21], that determines the FlyBS positions in real time by iteratively shifting the whole set of FlyBSs in the cell. In a single iteration, the power allocation is performed just once and then each FlyBS is shifted by a shift vector proportional to its current respective positioning net force. The proposed positioning solution that uses the established power allocation force field is described in Algorithm 1.

The algorithm starts with the assignment of the initial values (lines 1 to 4) for each FlyBS $j \in \mathbb{F}$ in the cell. Parameter c_j is a logical value representing a state of convergence of FlyBS j, that is whether the FlyBS has already converged to its given position or not, and α_j is a multiplicative factor that controls the magnitude of the positioning step shift, i.e. the distance by which the FlyBS is shifted towards its final position in the current iteration of the algorithm. Then, the positioning convergence loop itself starts (line 5). Each iteration of the convergence loop represents one positioning step. Within the iteration, first, the power allocation for the whole cell is performed according to Lemma 3 (line 6). Then, the next-step positions of all utilized FlyBSs are determined (lines 7 to 29). Note that only FlyBSs with at least one associated UE are repositioned, that is, only if $N_{UE}^{(j)} > 0$ (line 8).

For each FlyBS to be repositioned, the current overall net force is determined via (3.46) (line 9) and the first convergence condition is checked. If the magnitude of the net force is less than or equal to positioning precision ϵ, i.e., a threshold at which the magnitude is already considered close to zero, the repositioning of the given FlyBS is suspended, the logical value c_j is set to indicate that FlyBS j has converged to its current equilibrium position and the algorithm continues with the next FlyBS $j + 1$ (lines 10 to 12). Otherwise, the c_j convergence indication is set to false (line 14) and the current force vector is compared with the force vector of the previous positioning step. If the two vectors have a mutual angle difference of more than $\frac{\pi}{2}$, that is the force changed its direction by more than 90° compared to the previous step, the FlyBS is very probably close

to its final position. Then, utilizing the bisection method approach, the multiplicative factor α_j is divided by 2 (lines 16 to 21) [21]. This measure speeds up the convergence of the algorithm by cutting the distance the FlyBS is shifted each step in half every time the force changes to the opposite direction. To prevent the factor α_j from reaching very low values, which would eventually result in a close to none position shift that has an imperceptible effect on the power allocation, the bisection measure is applied only as long as α_j is higher than 1.

Algorithm 1 Positioning of the FlyBSs

1: **for** each j in $\mathbb{F}$ **do** ▷ initialize each FlyBS in the cell with starting values
2: $\alpha_j \leftarrow \alpha_{init}$, $\alpha_j^{(prev)} \leftarrow 0$
3: $\vec{F}_j^{(prev)} \leftarrow$, $c_j \leftarrow false$
4: **end for**
5: **while** (true) **do** ▷ positioning convergence loop start
6: Perform power allocation according to Lemma 3
7: **for** each j in $\mathbb{F}$ **do**
8: **if** $N_{UE}^{(j)} > 0$ **then** ▷ do not reposition FlyBSs with no UE assigned
9: Determine net force $\vec{F}_j$ applied to the FlyBS via (3.46)
10: **if** $|\vec{F}_j| \leq \epsilon$ **then** ▷ 1st convergence condition
11: $c_j \leftarrow true$
12: continue with the next FlyBS
13: **else**
14: $c_j \leftarrow false$
15: **end if**
16: **if** $|\vec{F}_j^{(prev)}| > 0$ **then**
17: $\beta \leftarrow \arccos\left(\frac{\vec{F}_j \cdot \vec{F}_j^{(prev)}}{|\vec{F}_j| \cdot |\vec{F}_j^{(prev)}|}\right)$
18: **if** $\beta > \frac{\pi}{2}$ and $\alpha_j > 1$ **then**
19: $\alpha_j \leftarrow \frac{\alpha_j}{2}$
20: **end if**
21: **end if**
22: **if** both $\alpha_j, \alpha_j^{(prev)} = 1$ and $\beta > \frac{\pi}{2}$ **then** ▷ 2nd convergence condition
23: $c_j \leftarrow true$
24: continue with the next FlyBS
25: **end if**
26: $\Delta\vec{r}_j \leftarrow$ Evaluate the reposition vector according to (3.47)
27: $r_{flybs,j} \leftarrow r_{flybs,j} + \Delta\vec{r}_j$ ▷ shift the FlyBS position
28: $\vec{F}_j^{(prev)} \leftarrow \vec{F}_j$, $\alpha_j^{(prev)} \leftarrow \alpha_j$
29: **end if**
30: **end for**
31: **if** $\forall j \in \mathbb{F}, c_j = true$ **then**
32: break
33: **end if**
34: **end while**

Given the behavioral characteristics of the positioning forces described in Section 3.2.2, in some cases it may happen that after several iterations of the algorithm the FlyBS reaches the position of the dominant source object (the BS or one of the UEs), that is the most power loaded one, and still not reach the equilibrium point, while further being "pulled" towards the dominant object by the net force. Such behavior can occur for example when the BS is heavily loaded by communication other than with the FlyBS j. Then, pulling the FlyBS towards the BS may not be enough to eliminate the power bottleneck the BS presents. Then, the BS remains fully loaded and the net force still points in the direction of the BS according to force definitions (3.44), (3.45) and (3.46). In such a case, the algorithm would fall into an infinite loop with the FlyBS "jumping around" the BS. To prevent this, the algorithm stops repositioning the FlyBS j when it registers such a loop and concludes that the FlyBS cannot get any closer to its desired target position (line 22). Then, the value c_j is set to indicate a successful convergence of the FlyBS position and the algorithm continues with the next FlyBS in the set. This marks the second convergence condition.

Finally, if none of the convergence conditions are satisfied, the FlyBS j is shifted by a reposition vector (line 27) determined as:

$$\Delta\vec{r_j} = \alpha_j \vec{F_j}, \tag{3.47}$$

where the individual elements of $\vec{r_j}$ denote a reposition difference in corresponding coordinates of the FlyBS position. Then, the current values of α_j and force $\vec{F_j}$ are stored for the next iteration (line 28). After the repositioning step is evaluated for each FlyBS, the final condition is checked. The whole loop ends when all of the FlyBSs in the cell have converged to an equilibrium position (line 32). This marks the end of the algorithm.

Even though every iteration of the algorithm introduces a change in the power allocation environment, which from the perspective of a single FlyBS step evaluation cannot be predicted as we do not know whether and where exactly would the other FlyBSs be repositioned in the current step, the algorithm still converges to a final and stable positioning solution after a finite number of iterations. This is thanks to the multiplicative factor α_j which dynamically decreases the magnitude of the positioning step for each FlyBS separately every time that FlyBS turns in the opposite direction. In addition, as the magnitude of the net force (3.46) cannot be generally higher than 1, parameter α_j determines the maximal distance, by which the FlyBS j can be shifted in one iteration according to (3.47). Hence, the parameter α_j is further denoted as the maximal positioning step.

Note that the algorithm is provided with two input parameters in total: initial maximal positioning step α_{init}, which adjusts the magnitude of every position shift, and the

tolerance ϵ that specifies the level at which the net force magnitude is considered close to zero. As the parameter ϵ determines the precision of the final positioning, it is further denoted only as positioning precision.

3.3 Association of UEs with the serving stations

In this section, the association of individual UEs to the serving stations is proposed. To this end, first, the association subproblem is formulated, and then, it is solved via implementing two heuristic algorithms dealing with initial association and association correction.

3.3.1 Association subproblem

The objective of the association is to maximize the minimal channel capacity, which after utilization of the proposed power allocation described in Section 3.1 translates to maximization of the common capacity C_i, while considering static positions of all objects, including the FlyBSs. Thus, the association subproblem is formulated as:

$$\begin{aligned} \boldsymbol{A}^* &= \underset{\boldsymbol{A}}{\operatorname{argmax}} \left(C_i\right) \\ s.t. \qquad (3.48a) \qquad & ||\boldsymbol{a_i}||, ||\boldsymbol{a_j^{(F)}}|| = 1, \quad \forall j \in \mathbb{F}, \\ (3.48b) \qquad & a_{j,b}^{(F)} = 1, \quad \forall j \in \mathbb{F}, \end{aligned} \tag{3.48}$$

where constraints (3.48a) and (3.48b) are the same as in (2.18) and restrict each of the FlyBSs to be associated only with the BS and all UEs and FlyBSs to be associated with exactly one serving station at a time.

As the association generally depends on the positions of serving stations which may not always be known, the association solution is split into two parts: initial association and its correction. The initial associations are determined via the means of UE clustering based on distances between objects, and thus, only serve as an initial estimation. Then, the association correction is achieved via reassociating certain UEs to different serving stations to further boost the common capacity, considering the positions of all serving stations are already known.

Note that to save time consumed by unnecessary reassociation of real network objects and to suppress uptime decrease of individual links caused by related unnecessary handovers, both association parts are executed virtually via the utilization of the path loss prediction described in Section 2.1.5, without any actual reassociation taking place. Then, only the final association is applied.

3.3.2 Initial association

As the FlyBS positions are generally unknown at the time of initial association, the association cannot be derived from actual object relations in the cell. On the other hand, the position generality does not apply to the UEs as they are considered static during association. Therefore, the associations are estimated via clustering the UEs based on their position into K sets, each to be served by a different serving station.

Choosing from an available set of clustering solutions while having an emphasis on keeping the complexity of the initial association as low as possible, the *k-means* algorithm stands as a reasonable candidate. The algorithm minimizes distances between objects in the cluster and its centroid, which is a property convenient for joint maximization of SINR, and thus channel capacity, that each serving station separately is able to provide for its associated set of downlink channels. However, due to the characteristics of the k-means and its behavior in the established system model, the algorithm in its original form is unfortunately not a suitable solution for the initial association. To combat the undesirable behavior of the conventional k-means clustering algorithm, a novel clustering solution is designed and proposed.

First, the function and characteristics of the conventional k-means algorithm are summarized, and then, the proposed modified algorithm is described.

K-means clustering algorithm

The conventional k-means algorithm is based on Euclidean distances between objects and the cluster centroids. The overall clustering process is summarized in the following 5 steps [29]:

(1) The algorithm starts with an initial set of artificial cluster centroids.

(2) The clusters are initialized by assigning each object in the system to the cluster with the nearest centroid, which is the centroid that has the lowest Euclidean $\mathbb{R}^2$ distance to the object in question.

(3) Having the initial clusters established, their real centroids are evaluated and stored.

(4) Then, the process is repeated: each object in the system is reassigned to the cluster with the nearest centroid.

(5) Following that, steps 3 and 4 are iteratively repeated until there is no change in the cluster assignment registered, i.e. no object is reassigned in the current iteration.

The stop condition in step 5 marks the end of the algorithm. Every single object is assigned to the cluster with the nearest centroid possible, and thus the sum of the distances between objects and their respective cluster centroids is minimized.

However, the conventional k-means algorithm presents a set of restrictions that make it inconvenient for deriving initial associations in the FlyBS-supported network. The major drawbacks are summarized in the following two observations:

1. The k-means algorithm minimizes distances between objects (UEs) and the cluster centroids, which would, without taking backhaul interference into account, stand as suitable positions for respective serving stations. However, the evaluated clusters are fully dynamic in terms of both the clustered set of UEs and its centroid. This property poses a problem for the BS, as its position is static, and thus not able to adapt to the dynamic cluster centroid, unlike the FlyBS. With the BS placed out of the cluster centroid, the cluster itself would not be fully utilized and the whole k-means distance minimization would be compromised. Therefore, the conventional k-means cannot be used for clustering the UEs with the BS, and thus allows utilization of only N_{FlyBS} clusters. However, excluding the BS from the cluster evaluation is also not a suitable solution, as this way all the UEs would be initially associated with the FlyBSs. Then, the BS would most probably be heavily underutilized in terms of power.

2. The conventional k-means uses only bare Euclidean distance for the determination of the clusters. Thus, the different transmission power budgets of different serving stations are not taken into account. Considering that the UEs could be initially associated with the BS contrary to point 1, this poses another problem. Firstly, all of the clusters including the BS are approximately comparable in terms of sums of distances, and secondly, it is considered that the BS has a much higher power budget than the FlyBS, and thus can operate under a much higher load. Then, this property of the k-means again leads to heavy under-utilization of the BS.

Modified k-means clustering for initial association

To combat the restrictions of the conventional k-means clustering algorithm described above, the following modifications are introduced. First, to allow UEs to be initially associated with the BS without compromising the desired distance minimization, the modified solution deploys an additional special cluster with a static centroid placed at the position of the BS. This method changes the way this particular cluster is evaluated compared to the conventional k-means procedure, as it is not derived by iterative minimization of distances to a floating centroid, but rather "built around" a static and constant centroid

defined prior to the association. Thus, this modification consists of adding the BS position to the initial set of cluster centroids and excluding this static cluster from the centroid reevaluation in step 3.

Secondly, in order to eliminate the initial power under-utilization of the BS, a weighing factor w for UE to BS distance evaluation is introduced. This allows for a modification, i.e., stretching or shrinking, of real Euclidean distances in the system, and as such enables control of the clustering result via adjusting the w variable. The distance between UE i and the BS is expressed as:

$$d_{i,b} = w||r_{ue,i} - r_{bs}||, \tag{3.49}$$

where operator $||.||$ denotes the evaluation of Euclidean distance. Then, the distance between UE i and FlyBS j is given as:

$$d_{i,j} = ||r_{ue,i} - r_{flybs,j}||. \tag{3.50}$$

Setting the weighing factor w with a value from continuous interval $\mathcal{W} = (0, ..., 1)$ artificially lowers all measured UE-to-BS distances, and thus results in more UEs to be initially associated with the more power-supplied BS. Then, each of the FlyBSs is associated only with the closest UEs, thus respecting the high BS-to-FlyBS power budget ratio.

The whole modified k-means clustering for initial association determination is described in Algorithm 2. Let the input parameters be a known matrix of UE $\mathbb{R}^2$ positions R_{UE} and a known desired number of clusters K, which is lower than or equal to the number of UEs in the cell. First, the initial cluster centroids for the first (K-1) FlyBS clusters are determined as a random permutation of UE position matrix R_{UE} (lines 1 to 3). The centroid set $\mathcal{C}$ is then appended by a static BS position r_{bs} (line 4).

After that, the cluster formation loop is initiated (line 6). Each iteration starts with determining the distances between UEs and the cluster centroids (lines 8 to 14). That is, for each UE i from the set of UE indices $\mathbb{U}$ a distance to every single centroid from the set $\mathcal{C}$ is evaluated either via (3.49) in case of the static cluster centroid (line 10) or (3.50) in case of a general dynamic FlyBS centroid (line 12). To determine the cluster association A, each UE is assigned to the cluster k that minimizes the evaluated distance $d_{i,k}$, that is a cluster with the nearest centroid (line 15). Then, if the reassignment of the set A leads to a different cluster association, new dynamic centroids $\{r_1, ..., r_{K-1}\}$ are evaluated based on the UE positions of each cluster (lines 18 to 20). Note that the static cluster centroid is not reevaluated here and stays the same for the whole course of the algorithm. Consequently, the current association A is stored for the next iteration (line

Algorithm 2 Modified k-means clustering

Ensure: R_{UE} is an N_{UE}-by-2 matrix of UE $\mathbb{R}^2$ positions
Require: cluster count $K \leq N_{UE}$
1: **for** each j in $\{1, ..., K-1\}$ **do**
2: $\quad \mathcal{C}(j) \leftarrow$ unique random position from R_{UE}
3: **end for**
4: $\mathcal{C}(K) \leftarrow r_{bs}$
5: $A^{(prev)} \leftarrow 0$
6: **while** (true) **do**
7: $\quad$ **for** each i in $\mathbb{U}$ **do**
8: $\quad\quad$ **for** each k in $(1, ..., K)$ **do**
9: $\quad\quad\quad$ **if** $k = K$ **then**
10: $\quad\quad\quad\quad d_{i,k} \leftarrow$ Evaluate distance to BS via (3.49)
11: $\quad\quad\quad$ **else**
12: $\quad\quad\quad\quad d_{i,k} \leftarrow$ Evaluate distance to FlyBS via (3.50)
13: $\quad\quad\quad$ **end if**
14: $\quad\quad$ **end for**
15: $\quad\quad A(i) \leftarrow \text{argmin}_k\,(d_{i,k})$
16: $\quad$ **end for**
17: $\quad$ **if** $A \neq A^{(prev)}$ **then**
18: $\quad\quad$ **for** each j in $\{1, ..., K-1\}$ **do**
19: $\quad\quad\quad \mathcal{C}(j) \leftarrow$ Evaluate new cluster centroid
20: $\quad\quad$ **end for**
21: $\quad\quad A^{(prev)} \leftarrow A$
22: $\quad$ **else**
23: $\quad\quad$ break
24: $\quad$ **end if**
25: **end while**

21). The loop ends when the association A stays unchanged in two consecutive iterations (line 23). This marks the end of the algorithm. The final clustering A is determined.

Finally, the proposed initial association utilizing the modified k-means clustering is described in Algorithm 3. The process starts with assigning the initial variables. The matrix R_{UE} with $\mathbb{R}^2$ positions of all UEs in the cell is composed (lines 1 to 3) and then the number of clusters K is derived (lines 4 to 8). As the k-means algorithm is designed to divide a set of N objects into a maximum of N clusters, the cluster count is limited by the number of UEs in the cell. If the restriction does not apply, the number of clusters K is equal to the number of available FlyBSs N_{FlyBS} plus 1 representing the BS (line 5). Otherwise, if the number of UEs N_{UE} is less than or equal to $N_{FlyBS} + 1$, only $K = N_{UE}$ clusters are deployed (line 7), where one of them is the static BS cluster and the rest (K-1) are the FlyBS clusters. Therefore, in such a case, only (N_{UE}-1) FlyBSs are deployed.

Then, the modified k-means clustering is performed via Algorithm 2, returning a cluster association set A, where each entry $A(i)$ marks the cluster k, which the UE i is associated with. Finally, after evaluating the clusters, each UE is associated with its respective cluster head, that is the BS in case of the cluster K, or FlyBS k in case of the cluster $k = \{1, ..., K-1\}$. At this point, the initial UE association is complete.

Algorithm 3 Initial UE association via modified k-means clustering

for each i in $\mathbb{U}$ **do**
    $R_{UE}(i) \leftarrow r_{ue,i}$
end for
if $N_{UE} > N_{FlyBS} + 1$ **then**
    $K \leftarrow N_{FlyBS} + 1$
else
    $K \leftarrow N_{UE}$
end if
$A \leftarrow$ Perform modified k-means clustering of N UEs into K clusters via Algorithm 2
for each i in $\mathbb{U}$ **do**
    if $A(i) = K$ **then**
        Associate UE i with the BS
    else
        Associate UE i with the FlyBS j, where $j = A(i)$
    end if
end for

3.3.3 Association correction

The objective of the correction is to improve the initial association performed via Algorithm 3 and further boost the common capacity, considering an already known set of FlyBS positions. As the common capacity is given by the power allocation bottleneck according to Section 3.1.5, the only way to further increase the capacity is to reassociate some UEs away from the fully loaded serving station. This way, the power load is shifted to a different serving station that is not yet fully utilized, relieving the bottleneck and enabling it to allocate more power to the remaining set-up downlinks, thus increasing the common capacity.

However, note that not all such reassociation attempts might lead to a capacity increase, as there is only a limited number of reassociation options, given the discrete distribution of FlyBS and UE positions. Therefore, a method of choosing the right UE to reassociate should be established. Furthermore, each reassociation leads to the change of system state, and thus requires a new power allocation to take place, which changes power relations in the whole cell. Considering this, it is not easy to determine whether a capacity increase can be expected or not prior to the reassociation, and thus an analytical solu-

tion is considered infeasible. Therefore, based on the described observations, a heuristic iterative algorithm finding a final association is described and proposed. In general, to increase the common channel capacity, the algorithm finds convenient reassociations via a "trial and error" method based on a defined reassociation metric, until no other possible reassociation results in a capacity increase. To describe the proposed correction solution more closely, first, the method of eliminating a single bottleneck is outlined, and then, it is expanded to an algorithm covering the whole association correction.

Elimination of the bottleneck

In order to decrease the complexity of the proposed bottleneck elimination, not all possible reassociations are tested, as sometimes it is already clear prior to the test that the reassociation would not benefit the system. Therefore, reassociation pairs, that is a particular UE and a promising target serving station, suitable for the test are chosen based on the reassociation metric. Thus, the metric determines the capacity benefit of associating the UE i to a given target T in comparison to the current state of the system and is defined as:

$$m_i^{(T)} = \delta P_T^{(left)} \frac{g_{i,T}}{g_{i,C}}, \tag{3.51}$$

where $P_T^{(left)}$ is the free, not utilized power budget of the target T, which denotes either a particular FlyBS or the BS. Then, parameter $g_{i,T}$ is the channel gain between UE i and the target, while $g_{i,C}$ is the gain of the channel between the UE and the serving station it is currently associated with. Finally, parameter δ is a devaluation term defined as:

$$\delta = \begin{cases} -1 & \text{if } (g_{b,T} - g_{i,b} < 0) \vee (g_{i,T} - g_{i,b} < 0), \\ 1 & \text{otherwise,} \end{cases}, \tag{3.52}$$

where $g_{b,T}$ is the channel gain between the target and the BS, while $g_{i,b}$ is the gain of the channel between UE i and the BS. Reassociation metric defined this way favors UEs with high path loss of the link between them and their current serving station, as reassociating such UE would result in a significant bottleneck relief. However, to prevent creating an even deeper bottleneck on the target serving station, the metric also takes characteristics of potential targets into account, that is, the target's available transmission power and the channel gain between the UE and the target. Additionally, satisfying the condition in (3.52) means that the pair is not beneficial, and thus, the parameter δ devaluates the metric by assigning it a negative value. This way, the pair is eliminated from the reassociation test to decrease the complexity. Specifically, the parameter δ prevents the following two cases:

(i) assigning the UE to the FlyBS, whose backhaul has a higher path loss than a link between the UE and the BS, as the BS would almost certainly have to allocate more power for the backhaul than the direct link to the UE, thus leading to capacity decrease,

(ii) assigning the UE to the FlyBS, with which the newly established access channel would have a higher path loss than the direct link to the BS, as this would again most probably lead to capacity decrease compared to the association with the BS.

Finally, an example of reassociation metric utilization is illustrated in Figure 3.5.

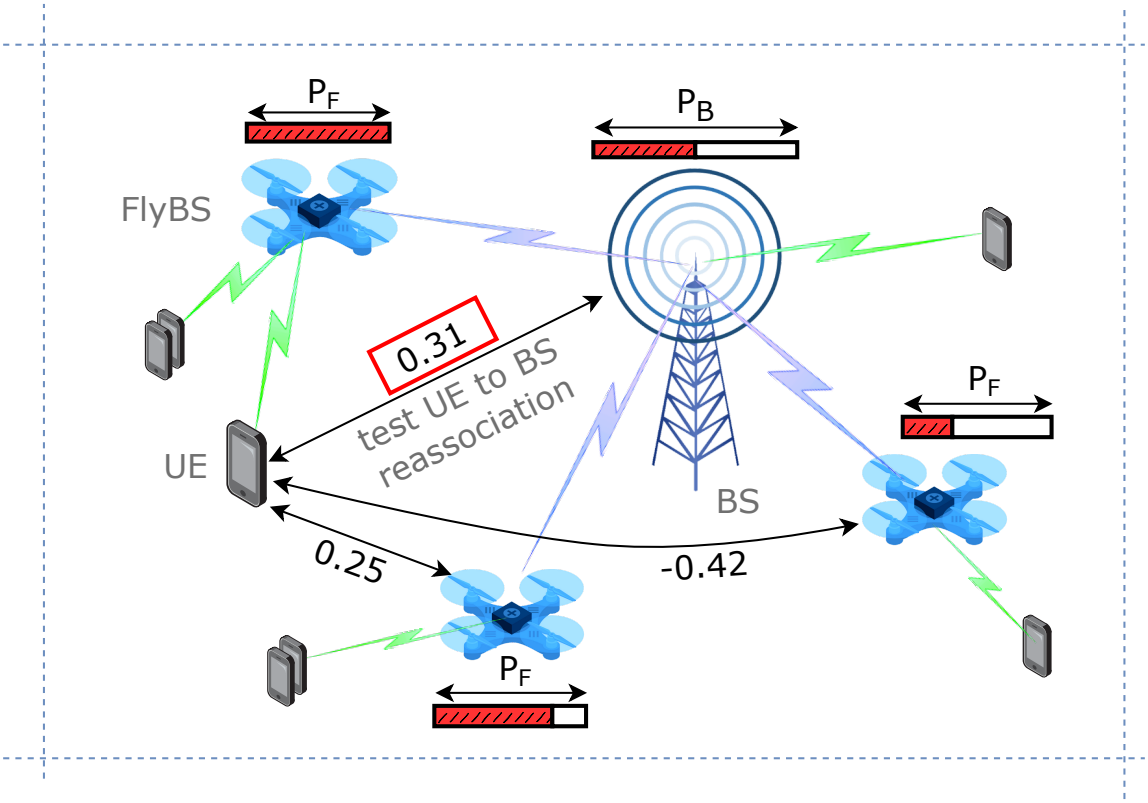

Figure 3.5: Illustrative example of reassociation metric utilization

Having the reassociation metric established, the whole bottleneck elimination process is described in Algorithm 4. The algorithm takes the current bottleneck obtained via (3.41) as input, after which the initial values, bottleneck elimination indication e and channel capacity, are assigned (lines 1 and 2). Then, a reconnection metric is evaluated according to (3.51) for every UE-target pair. That is, every UE i from the set of UEs associated with the bottleneck $\mathbb{U}_\beta$ evaluates a reassociation metric with each of the FlyBSs (line 5) and the BS (line 7). All metrics are stored in a matrix M of size $N_{UE}^{(\beta)} \times (N_{FlyBS}+1)$, where $N_{UE}^{(\beta)}$ is the number of UEs associated with the bottleneck. Each element (i, j) in columns 1 to N_{FlyBS} is a metric for UE i and target FlyBS j, while each element in the last column represents a metric for UE i and the BS pair.

Algorithm 4 Elimination of the bottleneck

Input: power allocation bottleneck b
1: $e \leftarrow false$
2: $C^{(prev)} \leftarrow$ Evaluate common channel capacity
3: **for** each i in $\mathbb{U}_\beta$ **do**
4: **for** each j in $\mathbb{F}$ **do**
5: $M(i,j) \leftarrow$ Evaluate metric with the FlyBS $m_i^{(j)}$ according to (3.51)
6: **end for**
7: $M(i, N_{FlyBS}+1) \leftarrow$ Evaluate metric with the BS $m_i^{(b)}$ according to (3.51)
8: **end for**
9: **while** (true) **do**
10: $m_{max} \leftarrow \max(M)$
11: $i,j \leftarrow \text{argmax}_{i,j}(M(i,j))$
12: **if** $m_{max} \leq 0$ **then**
13: break
14: **end if**
15: $a_i^{(prev)} \leftarrow a_i$ ▷ current association of UE i
16: $a_i \leftarrow$ Associate UE i with the target j
17: Perform new power allocation according to Lemma 3
18: $C^{(new)} \leftarrow$ Evaluate common channel capacity
19: **if** $C^{(new)} > C^{(prev)}$ **then**
20: $C^{(prev)} \leftarrow C^{(new)}$
21: $b^{(new)} \leftarrow$ Find power allocation bottleneck according to (3.41)
22: **if** $b^{(new)} \neq b$ **then**
23: $e \leftarrow$ true
24: break
25: **end if**
26: **else**
27: $a_i \leftarrow a_i^{(prev)}$
28: **end if**
29: $M(i,j) \leftarrow 0$
30: **end while**
Output: e ▷ indication of whether the bottleneck was successfuly eliminated

After the metric evaluation, the actual elimination loop is initiated (line 9). In each iteration, first, a maximal value of M is obtained together with its corresponding indices i and j (lines 10 and 11). If the maximum metric is lower than or equal to zero, it means that there is no option left to relieve the bottleneck via UE reassociation and the loop is broken (line 13). Otherwise, the reassociation of the obtained UE i to the most promising target j is tested. The current association of UE i is stored (line 15), and then, it is associated with target j, which is the BS if $j = N_{FlyBS} + 1$, or the FlyBS otherwise (line 16). Then, a new power allocation is performed and new channel capacity is evaluated (lines 17 and 18). If the new channel capacity is higher than the previous, the new association is kept and the previous capacity updated (line 20). Then, the current

bottleneck is obtained again via (3.41) (line 21). If the new bottleneck is the same as the previous one, the loop continues. However, if the new bottleneck is a different object, it means that the previous one was successfully eliminated, bottleneck elimination indication e is assigned with a true value, and the loop is broken (lines 23 and 24). Nevertheless, if the new channel capacity is not higher than the previous one, the previous association is restored (line 27). Finally, at the end of the iteration, regardless of the association decision, a zero value is assigned to the (i, j) element of the metric matrix M to prevent the pair from being tested again in the next iteration (line 29). All in all, the elimination loop ends when either there is no positive value left in M (line 13), or the bottleneck was successfully eliminated (line 24), after which the indication of elimination result e is returned as output. This marks the end of the bottleneck elimination algorithm.

Reassociation algorithm

Finally, the whole association correction utilizing an iterative method of bottleneck elimination is described in Algorithm 5. The algorithm starts with the correction loop initiation (line 1). In each iteration, first, the current power allocation bottleneck is found via (3.41) (line 2). Then, an attempt at the elimination of bottleneck b is performed via Algorithm 4 and an indication of whether it has been successful is returned (line 3). If the bottleneck has been successfully eliminated, the loop continues with the next iteration and tries to eliminate the next bottleneck in the system. However, if the bottleneck has not been successfully eliminated by Algorithm 4, the performed successful reassociations are retained, the loop is broken (line 5) and the association correction algorithm ends. As the current bottleneck cannot be eliminated, it continues to determine the common channel capacity for the whole cell, and thus, there is no other way left to increase the capacity via the means of UE reassociation.

Algorithm 5 Association correction

```
1: while (true) do
2:     b ← Find power allocation bottleneck via (3.41)
3:     e ← Perform elimination of bottleneck b via Algorithm 4
4:     if e = false then
5:         break
6:     end if
7: end while
```

3.4 Final joint solution

After each of the simplified subproblems to the ultimate problem (2.18) has been solved separately, the final joint solution combining the partial solutions is summarized. Thus, the final heuristic algorithm utilizing the designed power allocation, FlyBS positioning, and UE association is proposed and described in this section.

As the UE association is based on already determined FlyBS positions, while on the contrary the FlyBS positioning is determined by a static state of UE associations, a causality problem arises. To overcome this, first, the proposed initial association algorithm is used to determine initial UE associations without prior knowledge of the FlyBS positions, and then, the proposed FlyBS positioning and association correction are alternately repeated in this order, until a final stable state is achieved. Note that the algorithm is designed to be executed fully virtually to save time and resources. Thus, next to FlyBS positions and associations, also all performed power allocations are evaluated based on predicted channel gain.

The final joint solution is described in Algorithm 6. First, the starting FlyBS positions and associations are initialized. All FlyBSs are initially stationed at the BS (line 2) and their positions are stored in the set R (line 3). Then, the initial associations are determined by clustering of UEs via Algorithm 3 (line 5). After that, the main loop starts (line 6). In each iteration, first, the FlyBSs are relocated to their current sub-optimal positions, after which the associations are corrected based on the current configuration.

To guarantee convergence of the algorithm, neither of the two positioning and association stages cannot result in a capacity decrease. Association correction satisfies this condition, as the capacity is either increased via successful reassociation, or no successful reassociation takes place at all, leaving the capacity unchanged. However, due to the random character of path loss prediction error, the positioning of FlyBSs may sometimes lead to a decrease in capacity. This is especially true when the positioning algorithm results in a very low distance shift of a certain FlyBS and the resulting path loss prediction error is higher than the actual propagation loss suppressed by the shift. In such a case, even though the propagation loss of a certain link is supposed to decrease by moving in a given direction, it actually increases due to the error.

To overcome this issue, first, the current common capacity is evaluated (line 7). Then, the positioning of FlyBSs via Algorithm 1 is executed, however, its resulting positions are stored only in a temporary variable (line 8). Consequently, the power allocation is evaluated and stored in a temporary variable too (line 9), after which the current channel capacity is determined again (line 10). If the new capacity is higher than or equal to the previous one, the new positions and power allocation are assigned to the actual position set R and power allocation set P, respectively (lines 12 and 13). Otherwise,

the newly obtained positions and power allocation are discarded. Then, the association correction is performed via Algorithm 5, after which an indication of whether at least one reassociation was successfully executed is returned (line 15) and the power allocation is determined again (line 16). Successful reassociation changes the state of the system, and thus, new FlyBS positioning has to be performed. The loop continues with the next iteration. However, if no successful reassociation is executed, the state of the system stays unchanged and the subsequent repositioning of the FlyBSs would result in the exact same positions as before. Hence, no further capacity increase is possible and the loop is broken (line 18). At this point, the obtained association, positioning, and power allocation are applied.

Algorithm 6 Final algorithm

1: **for** each $j \in \mathbb{F}$ **do**
2: $r_{flybs,j} \leftarrow r_{bs}$ ▷ $\mathbb{R}^2$ positions, that is only x, y coordinates
3: $R(j) \leftarrow r_{flybs,j}$
4: **end for**
5: Perform initial association via Algorithm 3
6: **while** (true) **do**
7: $C^{(prev)} \leftarrow$ Evaluate common channel capacity
8: $R^{(new)} \leftarrow$ Perform FlyBS positioning via Algorithm 1
9: $P^{(new)} \leftarrow$ Perform power allocation based on $R^{(new)}$
10: $C^{(new)} \leftarrow$ Evaluate common channel capacity based on $P^{(new)}$
11: **if** $C^{(new)} \geq C^{(prev)}$ **then**
12: $R \leftarrow R^{(new)}$
13: $P \leftarrow P^{(new)}$
14: **end if**
15: $x_a, A \leftarrow$ Perform association correction via Algorithm 5
16: $P \leftarrow$ Perform power allocation according to Lemma 3
17: **if** $x_a = false$ **then** ▷ no successful reassociation performed
18: break
19: **end if**
20: **end while**
Output: A, R, P

Chapter 4

System performance

In this chapter, the performance of the proposed joint power allocation, FlyBS positioning, and UE association is evaluated via a set of simulations. To this end, first, the simulation model and competitive schemes utilized for comparison are described. Then, the analysis of the proposed solution's parameterization is conducted via adjustment of the variable parameters, after which the final simulation results are presented against the competitive schemes. Finally, the performance of the multihop relay is evaluated based on a simplified scenario.

4.1 Simulation model description

The performance of the designed network is evaluated via a MATLAB simulation, in which the solution proposed in Chapter 3 is implemented. The system space and parameters describing the radio channels are assigned based on a general 5G RAN [30]. Therefore, a reference cell of dimensions 1000×1000 m with a single BS stationed in the middle is considered. The total of $N_I = 4$ neighboring BSs are deployed to provide inter-cell interference. Two of them are stationed 1100 m away from the reference cell BS in both directions of the x axis, while the other two are 1100 m away in both directions of the y axis. The described configuration is illustrated in Figure 4.1. Based on the 5G specification [30], the utilized bandwidth B is set to 400 MHz and the communication frequency f is fixed at 39 GHz. Then, the available power supply of the BS and each of the FlyBSs is $P_B = 38$ dBm and $P_F = 20$ dBm, respectively. To simulate a thermal noise, the considered noise spectral density is based on estimated average temperature $T = 283.15$ K and evaluated as $\sigma = 4KT = -198$ dBm/Hz, where K is the Boltzmann constant. Furthermore, altitudes of respective network objects' radio interfaces are estimated as follows: 20 m for the BS, 50 m for each FlyBS, and 1.5 m for a general UE. The established access network parameters are summarized in Table 4.1.

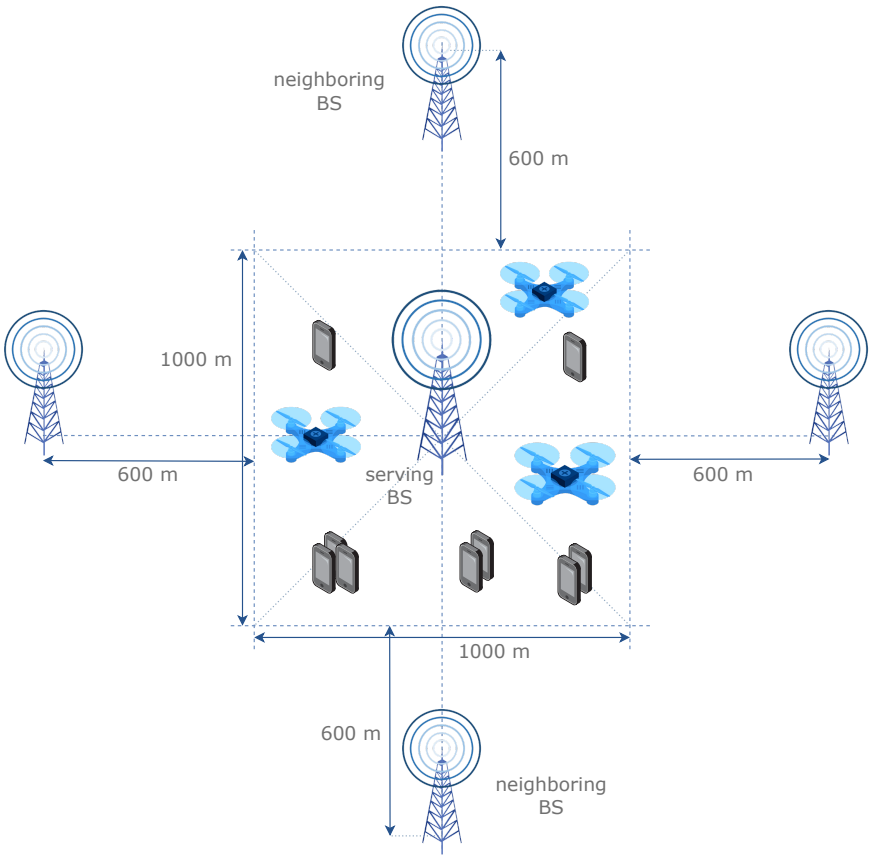

Figure 4.1: Illustration of the simulation model

Table 4.1: Overview of the simulated network's parameters

parameter	**value**	**description**
carrier frequency f	39 GHz	center of the communication band
bandwidth B	400 MHz	cell's total bandwidth
BS power budget P_B	38 dBm	total downstream transmission power available at the BS
FlyBS power budget P_F	20 dBm	total downstream transmission power available at each of the FlyBSs
BS z coordinate z_{BS}	20 m	altitude of the BS radio interface
UE z coordinate z_{UE}	1.5 m	estimated average altitude of the UE
FlyBS z coordinate z_{FlyBS}	50 m	altitude of the FlyBS operation
cell dimensions x_c, y_c	1000 × 1000 m	dimensions of the reference cell area $x_c \times y_c$
noise spectral density σ	-198 dBm/Hz	noise spectral density expressed as $\sigma = 4KT$

As the positions of UEs are according to Section 2.1.1 general, they are generated uniformly across the whole reference cell area. Thus, the x and y coordinates of each UE are generated randomly from uniform distributions $\mathcal{U}(0, x_c)$ and $\mathcal{U}(0, y_c)$, respectively. For a given configuration, the simulation is repeated over 400 drops, each with a different set of UE positions, over which the final presented results are averaged out. The simulations are executed under multiple configurations adjusting the number of UEs, deployed FlyBSs, and in case of the parameterization analysis also variable parameters of the proposed scheme. These are the initial maximal positioning step α_{init} and positioning precision ϵ used for FlyBS positioning described in Algorithm 1, and the weighing factor w utilized for initial association according to (3.49) and Algorithm 2. The variable parameters used in the simulations are together with their particular values or ranges summarized in Table 4.2. During parameterization analysis, multiple values from ϵ, α_{init} and w ranges are tested, while for the final simulations only specific static values determined by parameterization analysis are used.

Table 4.2: Overview of variable parameter settings for the simulations

parameter	**values**	**description**
number of UEs N_{UE}	20 to 100	total number of UEs in the reference cell area
number of FlyBSs N_{FlyBS}	2 to 20	total number of FlyBSs deployed in the reference cell
positioning precision ϵ	10^{-3} to 1	value of the positioning net force (3.46) that is already considered close to zero (Algorithm 1)
maximal positioning step α_{init}	15 to 300 m	initial value of parameter α_j that modifies the magnitude of FlyBS j shift according to (3.47) (Algorithm 1)
weighing factor w	10^{-3} to 1	value that modifies the evaluated distance between the UE and the BS during initial association (Algorithm 3)

In the final simulations, the proposed solution is compared against the two following competitive schemes, each configured according to Table 4.1:

- A scheme based on conventional k-means clustering of UEs for both FlyBS positioning and association. Each cluster of UEs is initially associated with one of the FlyBSs, which is positioned in the centroid of the respective cluster. Thus, no UE is directly associated with the BS. However, as the BS has a much higher available power supply than the FlyBS, this association is highly inefficient. Therefore, each

UE that is closer to the BS than the FlyBS it is associated with, is consequently reassociated to the BS, increasing the capacity of that UE. The scheme utilizes a fair power allocation, where each link managed by a certain serving station is allocated the same portion of that station's total power budget.

- The backhaul-aware scheme described in [20], which optimizes the power efficiency via power allocation at the FlyBSs and their positioning. The transmission power for individual access links is allocated to match the backhaul capacity so that neither the access nor the backhaul link would serve as a bottleneck. Note that the power allocated for both backhaul links and direct links between UEs and the BS is static and each of them is allocated the same portion of the total available power budget P_B. The scheme utilizes a joint power allocation and association solution, where the UE is associated with the serving station offering the highest capacity. The UE is associated with the FlyBS only if the FlyBS has enough power resources to match the access capacity with the backhaul. Therefore, to improve the association, the order in which the individual UEs test their association with the individual FlyBSs is given by the power efficiency metric. The metric is defined as the capacity gain to the required transmission power ratio. Finally, after the association, the positions of FlyBSs are corrected to fully utilize their available power supply.

Additionally, to illustrate the performance of the proposed solution in a real network, the scheme virtualization is simulated via the means of path loss prediction according to Section 2.1.5. The channel gain is evaluated according to (2.6), where the prediction error Φ is generated from a normal distribution with standard deviation of 1 dB, that is $\Phi = \mathcal{N}(0, 1)$, based on [27]. Thus, the whole final configuration consisting of FlyBS positions, UE associations, and power allocation is evaluated based on predicted values. Then, as the path loss prediction is no longer necessary after applying the configuration in the real network, the final results are obtained based on channel gain not burdened with the prediction error, that is according to (2.5).

To examine the performance of possible multihop relay utilization, a special simplified scenario is considered. A group of $N_{UE} = 10$ UEs is uniformly distributed in an area 200×200 m within the reference cell, where the distance between the area's centroid and the BS is R_T. A total number of N_{FlyBS} FlyBSs is deployed to serve the UEs via forming the multihop relay between the UEs and the BS. Thus, all UEs are associated only with one of the FlyBSs and the rest forwards the communication to the BS as part of the multihop. The utilized FlyBSs are evenly distributed on the line connecting the BS and the centroid of the UE area, equally spaced from each other. That is, the distances between the UE centroid and the first FlyBS, the last FlyBS and the BS, and distances

between each two associated FlyBSs are all the same and equal to $R = R_T/(N_{FlyBS} + 1)$. The power resources are evenly distributed among all UEs so that each access channel and each backhaul link forwarding the communication to a particular UE is allocated the transmission power equal to P_F/N_{UE}. As the multihop performance is significantly affected by the interference among individual members of the multihop relay, it is examined based on two different carrier frequencies f and multiple distances R_T. To illustrate the differences between the multihop utilization in the mid-band and millimeter-wave band, the frequencies used are 3.5 and 39 GHz. The considered multihop scenario is illustrated in Figure 4.2 and its parameterization is summarized in Table 4.3. To conclude the multihop specification, the capacities experienced by each of the UEs are evaluated according to (2.17) and (2.16).

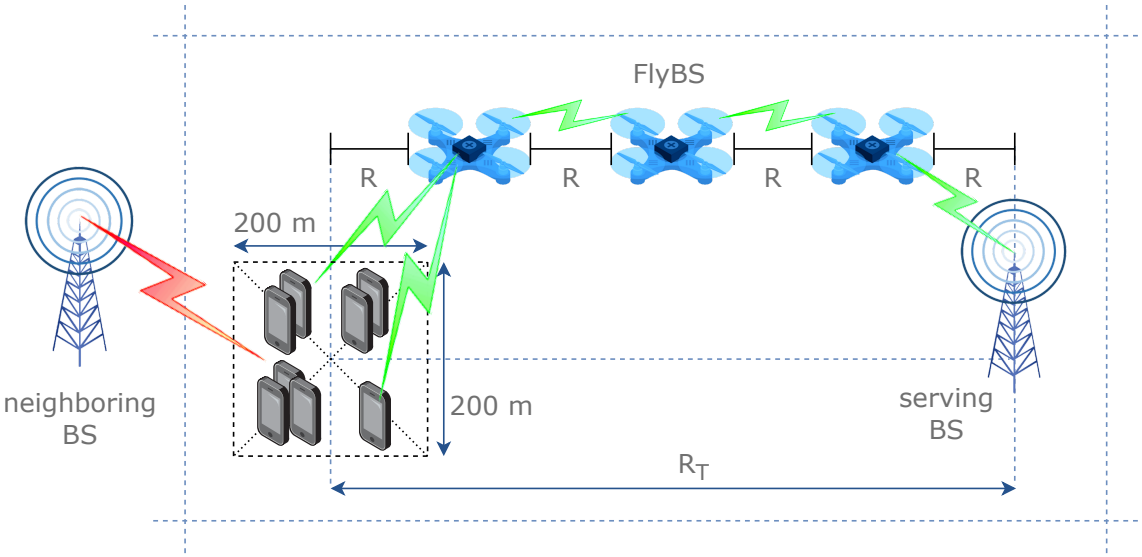

Figure 4.2: Illustration of the considered multihop scenario

Table 4.3: Overview of parameters of the multihop scenario

parameter	**values**
number of UEs N_{UE}	10
number of FlyBSs N_{FlyBS}	1 to 10
distance between the UEs and the BS R_T	100 to 400 m
carrier frequency f	3.5 and 39 GHz

4.2 Analysis of the scheme's parameterization

The purpose of the analysis is to examine the impact of the proposal's variable parameters on the overall performance and determine suitable values of positioning precision ϵ, initial maximal positioning step α_{init} and weighing factor w for the final performance evaluation. Individual values are determined to maximize the performance of the proposed scheme while keeping the complexity of the solution as low as possible at the same time. The complexity is evaluated based on the number of iterations of individual algorithms. Firstly, the total number of whole algorithm iterations, that is iterations of the final Algorithm 6, required to achieve convergence is examined. Secondly, as an iteration of Algorithm 6 is split into two stages, FlyBS positioning and association correction, an average number of each of the stage's iterations is also evaluated. One iteration of the positioning stage is defined as one iteration of Algorithm 1, where each of the FlyBSs is shifted by the current reposition vector, that is one positioning step marked by lines 5 to 30. Then, one iteration of the association stage is given by lines 9 to 30 of Algorithm 4, that is one iteration of the bottleneck elimination, where a reassociation of a single given UE-target pair is tested. Note that the defined iterations of individual stages are not comparable neither in computational complexity nor execution time. They serve only as mutually independent metrics of the complexity. In addition, based on the objective of the thesis, the overall performance of the scheme is evaluated via minimal and sum capacities.

As the parameters ϵ, α_{init} and w are interrelated via Algorithm 6 and their suitable values that achieve the maximal performance are mutually dependent on each other, setting those jointly proves difficult. Therefore, each of the parameters is examined separately, while keeping the other two assigned with a constant value according to Table 4.4. Hence, the final determination of the parameter values is not optimal and serves only as an estimation. All in all, a total of three separate simulations are conducted for the analysis. Each of the simulations adjusts one of the parameters ϵ, α_{init} and w within the range specified in Table 4.2. Then, its effect on the overall performance of the system is examined and the final value of the respective parameter is chosen. The simulations are executed with various numbers of UEs in the cell and a fixed number of $N_{FlyBS} = 6$ deployed FlyBSs.

Results of the positioning step analysis are illustrated in Figures 4.3 and 4.4. The first two Figures 4.3a and 4.3b show the effect of initial maximal positioning step α_{init} on the minimal capacity among UEs and the sum capacity of the system, respectively. The minimal capacity is not influenced by the positioning step at all and thus is not relevant for the analysis. On the other hand, for all examined UE numbers, the sum capacity increases slightly with the increasing maximal positioning step to the value of approximately 200 m, after which a gradual decrease is observed. Although this behavior might seem unexpected, it is in fact caused by the inaccurate positioning given by the

Table 4.4: Overview of constant parameter values for parameterization analysis

parameter	value
positioning precision ϵ	0.05
maximal positioning step α_{init}	50 m
weighing factor w	0.05
number of FlyBSs N_{FlyBS}	6

positioning precision value $\epsilon = 0.05$. The actual final position of the FlyBS lies in an interval around the suboptimum, where the positioning net force (3.46) is only lower than or equal to 0.05. Thus, the ϵ parameter cannot determine the actual positioning precision under a tolerance level of 0.05. Hence, based on the presented sum capacity results, it is apparent that a suitable setting of the maximal positioning step α_{init} corrects the positioning beyond the capabilities of the ϵ parameter. However, the overall effect of α_{init} on the sum capacity is minimal, as setting of the parameter according to Figure 4.3b modifies the capacity only within 1% of the maximal value for all of the examined numbers of UEs.

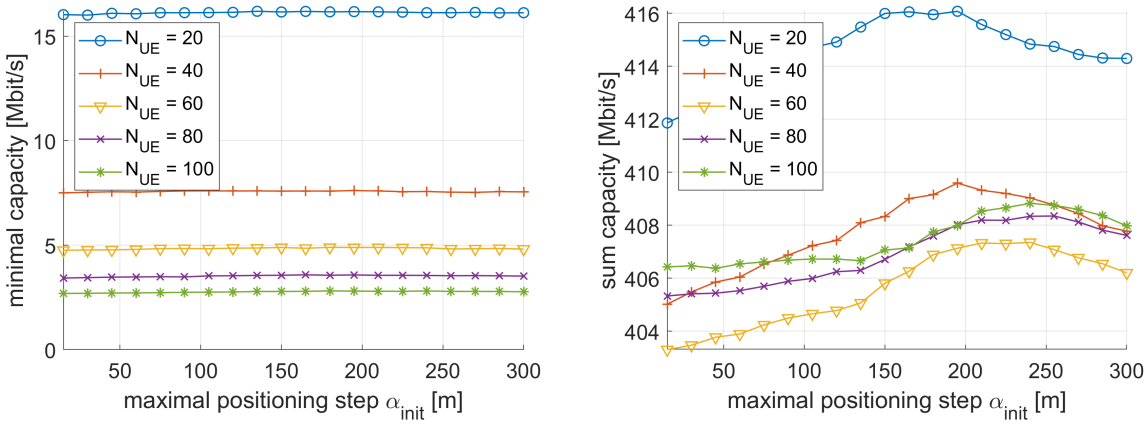

(a) minimal capacity (b) sum capacity

Figure 4.3: Channel capacity depending on initial maximal positioning step α_{init}, positioning precision $\epsilon = 0.05$, weighing factor $w = 0.05$

Then, in Figures 4.4a, 4.4b and 4.4c the dependence of the number of positioning stage, association stage and whole algorithm iterations on parameter α_{init} is illustrated. The number of positioning iterations generally decreases with the increasing positioning step for all UE counts as expected. However, three separate anomalies are observed for each of the UE counts, namely for positioning step values 75, 130, and 270 m. These anomalies are again caused by the imprecise positioning and can be suppressed by setting a lower value of ϵ. In addition, the minimal number of iterations increases with the

increasing number of UEs in the cell up to 60. This is caused by the initial positioning, that is, the first positioning stage after the initial association. With the higher number of UEs in the cell, more of them are initially associated with individual FlyBSs, and thus the FlyBS's suboptimal position lies closer to the associated UEs. Hence, the FlyBS has to cover a greater distance during initial positioning, thus resulting in more positioning steps. Nevertheless, neglecting the step anomalies, the number of positioning iterations stays approximately the same from $\alpha_{init} = 50$ m upwards for all of the UE counts. Thus, it is concluded that setting the positioning step within the range from 50 to 300 m generally does not affect the positioning stage convergence.

On the other hand, the positioning step α_{init} has a significant effect on the number of association iterations as illustrated in Figure 4.4b. For UE counts higher than 60, the number of iterations decreases with the increasing positioning step α_{init} up to the value of approximately 200 m, after which the number slightly increases. However, the number

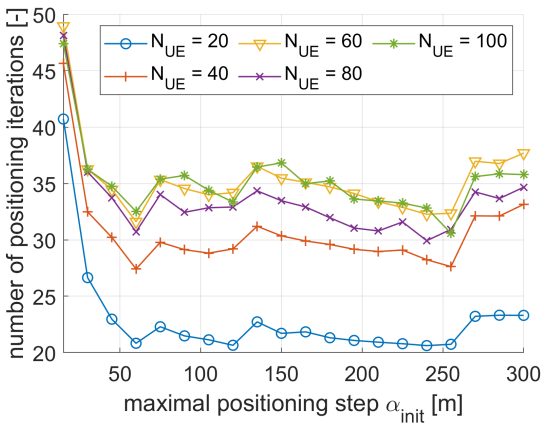

(a) positioning iterations

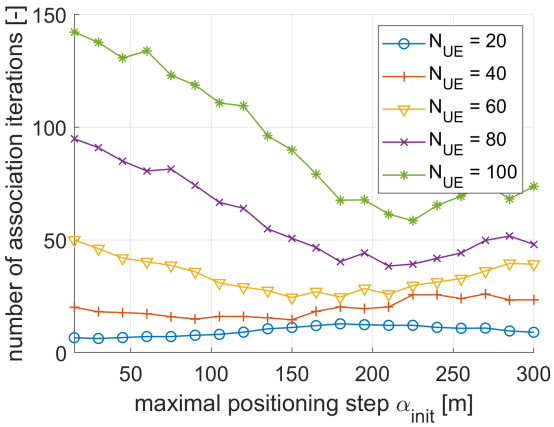

(b) association iterations

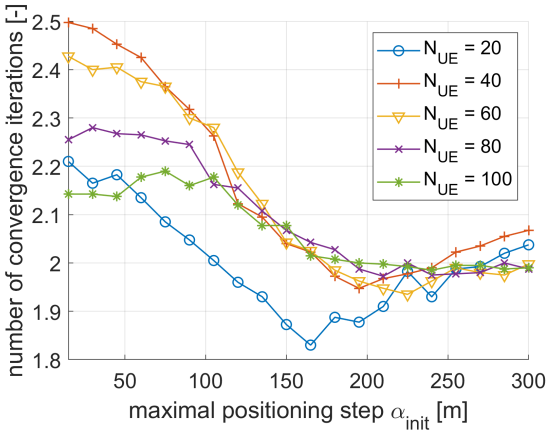

(c) whole algorithm iterations

Figure 4.4: Number of algorithm iterations depending on initial maximal positioning step α_{init}, positioning precision $\epsilon = 0.05$, weighing factor $w = 0.05$

of iterations for UE counts 20 and 40 almost doesn't change and slightly increses towards $\alpha_{init} = 200$ m, contrary to higher UE counts. This is again due to the significant difference in the number of UEs associated with single FlyBS. Nevertheless, as the iteration counts for N_{UE} values 20 and 40 are really low compared to N_{UE} values 80 and 100, their results are neglected as they are not that relevant for the determination of the final α_{init} value. Therefore, considering only values for UE counts 60 and higher, note that the individual iteration count minimums correlate with the sum capacity maximums in Figure 4.3b. This is due to the fact that the reassociation corrects the inaccurate positioning to a certain degree. Therefore, setting a less suitable value of α_{init} results in more association iterations needed to cover the inaccuracy. However, it is not possible to fully correct the positioning error, as there is only a limited set of discrete reassociation options available. This validates the observed sum capacity decrease in Figure 4.3b when $\alpha_{init} \neq 200$ m.

The whole algorithm iteration count dependence on α_{init} illustrated in Figure 4.4c shows a similar behavior to the number of association iterations. The reasons for this are the same as described above. That is a repetitive attempt of the association stage to correct the positioning error. Interesting is that the iteration count increases with decreasing number of UEs. This is because the higher amount of positioning constraints introduced by more UEs associated with a single FlyBS results in more precise positioning in one positioning stage, and thus decreases the probability the next whole algorithm iteration is necessary. The only anomaly in Figure 4.4c is the iteration count for $N_{UE} = 20$, which shows much lower values. This is most probably due to the fact that most of the FlyBSs serve only one UE, which is the least complicated scenario for positioning, as the FlyBS can only be stationed on a straight line between the UE and the BS. Finally, based on Figures 4.3b, 4.4b and 4.4c, the final suboptimal value of α_{init} is estimated as 200 m, and thus the analysis of maximal initial positioning step is concluded.

Consequently, results of the positioning precision analysis are illustrated in Figures 4.5 and 4.6. Figure 4.5a shows the dependence of the minimal capacity among UEs on positioning precision ϵ. For all UE counts, the minimum stays approximately the same up to the value of $\epsilon = 2 \cdot 10^{-2}$, after which the minimal capacity slightly decreases with increasing positioning precision. The behavior of the minimal capacity more or less correlates with the sum capacity illustrated in Figure 4.5b, where a graduate decrease with increasing ϵ is observed for all numbers of UEs. This is obvious as the lower the precision of FlyBS positions, the worse suppressed the power allocation bottleneck, and thus also the lower channel capacity. However, the decrease of the capacity is much more significant for lower numbers of UEs, as the FlyBS with more associated UEs has a lower degree of freedom during positioning, which compensates for a low positioning precision.

Additionally, for low UE counts in Figure 4.5b, a significant slowdown of the capacity decline with increasing ϵ is observed from positioning precision values of approximately 10^{-1} to $3 \cdot 10^{-1}$. The FlyBS positions are so inaccurate that it is more convenient to reassociate more of the UEs to the BS, thus compensating for the effect of the positioning error and slowing down the decrease. Note that the same behavior applies also for higher UE counts, but the overall decline is too slow for this to be apparent. Then, for positioning precision values approaching 10^0, a significant drop in sum capacity is observed for all of the UE counts. Although almost all of the UEs are reassociated to the BS, no compensation via reassociation is achieved as the FlyBSs are almost unutilized and the network behaves as if almost no FlyBSs were deployed. Thus the low channel capacity. Moreover, note that for more precise positioning, the lower UE counts perform better in terms of sum capacity. This is again due to the fact that in the case of fewer UEs associated with a single FlyBS, the FlyBS is positioned closer to the BS increasing the backhaul capacity.

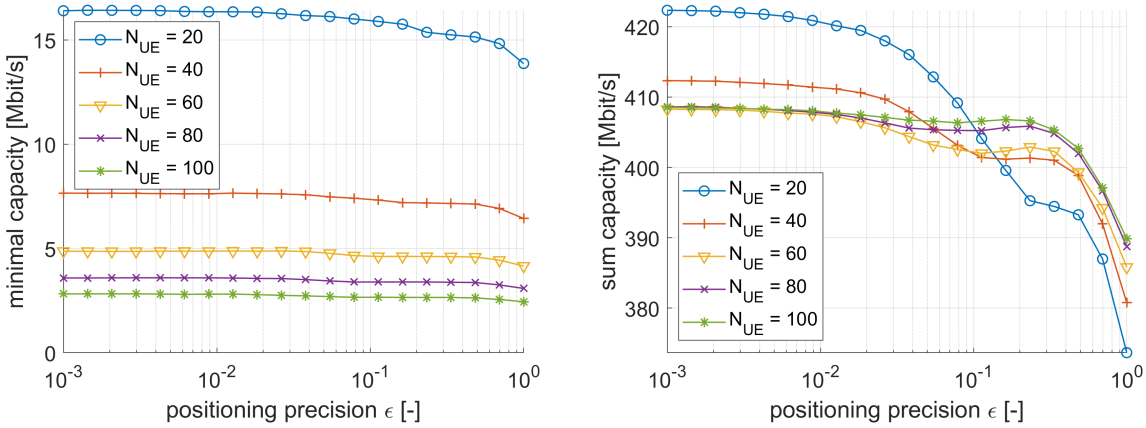

(a) minimal capacity (b) sum capacity

Figure 4.5: Channel capacity depending on positioning precision ϵ, maximal initial positioning step $\alpha_{init} = 50$ m, weighing factor $w = 0.05$

Figure 4.6a illustrates the dependence of number of positioning iterations on positioning precision ϵ. The iteration count decreases as expected, as the lower the precision the fewer positioning iterations are necessary to achieve convergence. Up to approximately $N_{UE} = 60$ the iteration count increases with higher number of UEs. This is again due to the FlyBSs being positioned farther away from the BS, resulting in more positioning iterations necessary after the initial association. Then, the number of association iterations is shown in Figure 4.6b. Note that for all examined UE counts the observed local maximums match the ϵ values, where similar anomalies are present in sum capacity in Figure 4.5b. The first local maximum of the association iteration count is observed approximately around $\epsilon = 10^{-1}$, where the reassociation stage successfully compensates for

the positioning error. Then, the second maximum lies at $\epsilon = 1$. This is due to the fact that most of the UEs are reassociated to the BS as a result of significantly inaccurate FlyBS positioning.

Finally, let's examine the number of whole algorithm iterations illustrated in Figure 4.6c. Note that if any UE is reassociated in the association stage, at least one additional whole algorithm iteration is necessary to correct the FlyBS positions according to the new association. Therefore, the iteration count can be lower than 2 only if no reassociation is conducted, that is both initial association and positioning precision are that precise. This is the reason why the iteration count increases with decreasing positioning precision, as the association correction results in more and more UE reassociations. Then, for all numbers of UEs, the iteration counts fall towards approximately the same value of 2.2 with ϵ approaching 1. This is again due to most of the UEs being reassociated to the BS in the first iteration, and as the subsequent repositioning is executed only for utilized FlyBSs,

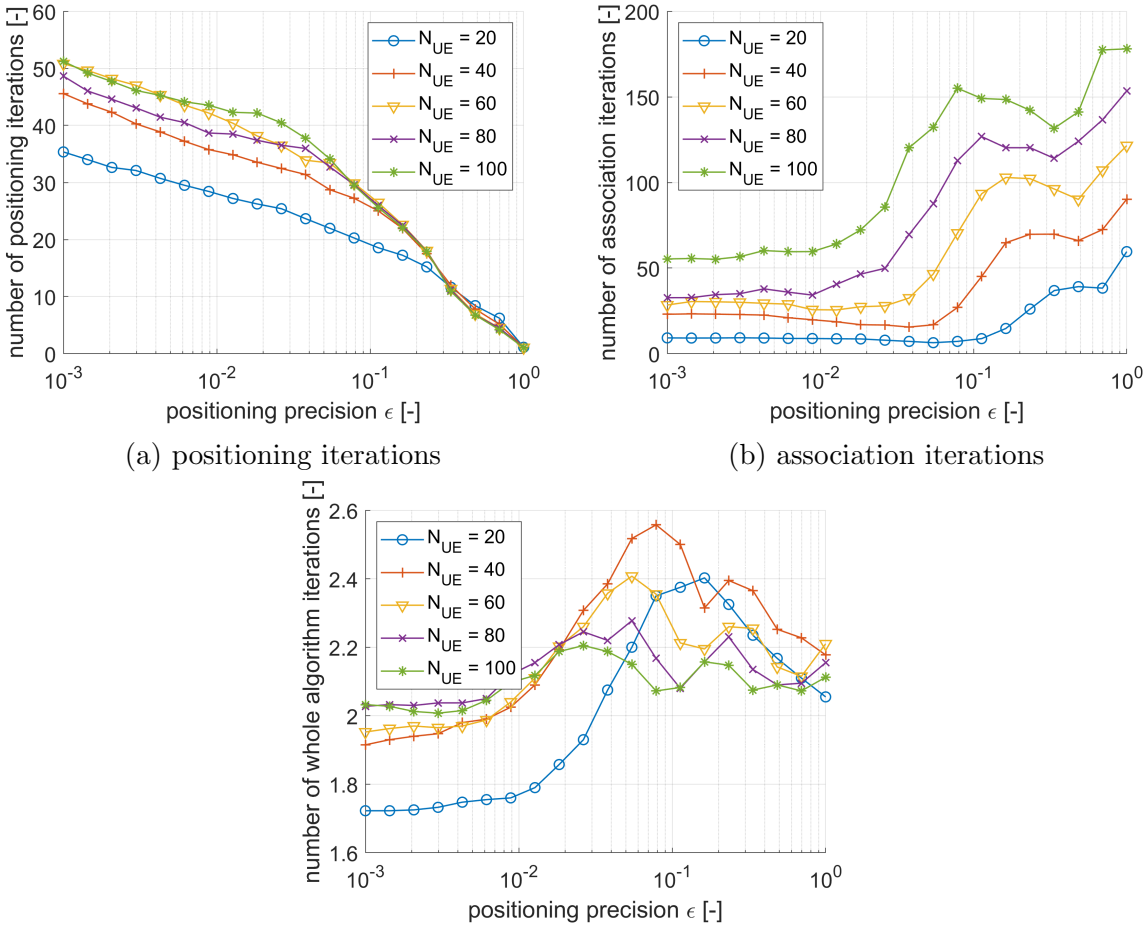

(a) positioning iterations

(b) association iterations

(c) whole algorithm iterations

Figure 4.6: Number of algorithm iterations depending on positioning precision ϵ, maximal initial positioning step $\alpha_{init} = 50$ m, weighing factor $w = 0.05$

the algorithm ends with the second iteration. However, for examined UE numbers 40 and higher, the iteration count peak around $\epsilon = 10^{-1}$ is disturbed by a local minimum, which lies in the same ϵ interval, where the increasing positioning error is being successfully compensated by reassociation as observed in Figure 4.5b. Then, according to the sum capacity, the reassociation stage results in the most significant capacity increase in this interval, and thus, the capacity most probably cannot be further exceeded by subsequent iteration. Hence, the algorithm converges in a lower number of iterations. This anomaly is not observed in the case of 20 UEs in the cell, as there is a really low number of reassociation options available due to only one or two UEs being associated with a single FlyBS.

To conclude the positioning precision analysis, let's compare the complexity and performance results. In terms of minimal and sum capacity, the acceptable values of positioning precision lie in the interval $\langle 10^{-3},\ 2 \cdot 10^{-2} \rangle$. Then, based on Figures 4.6b and 4.6c, the iteration counts are minimized for ϵ values lower than 10^{-2}. Note that the number of positioning precision iterations is not that relevant, as its peak is approximately 3x lower than association iteration count peak. However, in order to keep complexity of both of the stages as low as possible, the final positioning precision value is set as $\epsilon = 10^{-2} = 0.01$.

To find a suitable value of weighing factor w, let's examine Figures 4.7 and 4.8 presenting the dependence on the parameter. Figure 4.7a illustrates that the minimal capacity is almost unaffected by the weighing factor. The performance dependence is only apparent from the sum capacity illustrated in Figure 4.7b. The results show that the overall capacity of the system depends on the initial association and a suitable value w, that maximizes the capacity, can be found for each UE count separately. The reason for this is that the association correction method implemented in Algorithms 4 and 5 is not optimal, and thus, an inconvenient initial association cannot be fully corrected via reassociation. In order to lower the complexity, the proposed bottleneck elimination technique is equipped with only a limited set of tools for reassociation. That is, for example, an association of two UEs, where each of them is associated with a different serving station, cannot be switched in a single iteration. This is a non-negligible limitation, as the association swap via two consecutive iterations may not be possible due to power constraints.

For lower values of w, the sum capacity in Figure 4.7b decreases with increasing number of UEs in cell, until it saturates at around $N_{UE} = 60$. This is due to the following reason. Almost all of the FlyBSs initially serve only a very low number of UEs, that is one or two, whereas most of them are associated with the BS. Then, to relieve the BS bottleneck, the FlyBSs are pulled towards the BS during positioning. In some cases, this may result in the FlyBS reaching the BS position, while still not utilizing all of its power resources. Then, as the FlyBS hovers right above the BS, UEs from all directions can

be reassociated from the BS bottleneck to the FlyBS, thus locking it in position. This way, the FlyBS remains not fully utilized and the overall capacity is lower. However, note that this does not apply for lower numbers of UEs, as the BS initially serves less of them directly, leaving more power resources for backhaul links. On the other hand, for higher values of w, the sum capacity decreases with decreasing number of UEs. Nevertheless, this is due to a similar reason, as the majority of UEs are served by the FlyBSs. Then, the FlyBS is pulled towards its associated cluster of UEs. In some cases, it may reach a point, where no further position shift is possible, as the individual UEs try to pull the FlyBS in opposite directions. Thus, the FlyBS again remains not fully utilized.

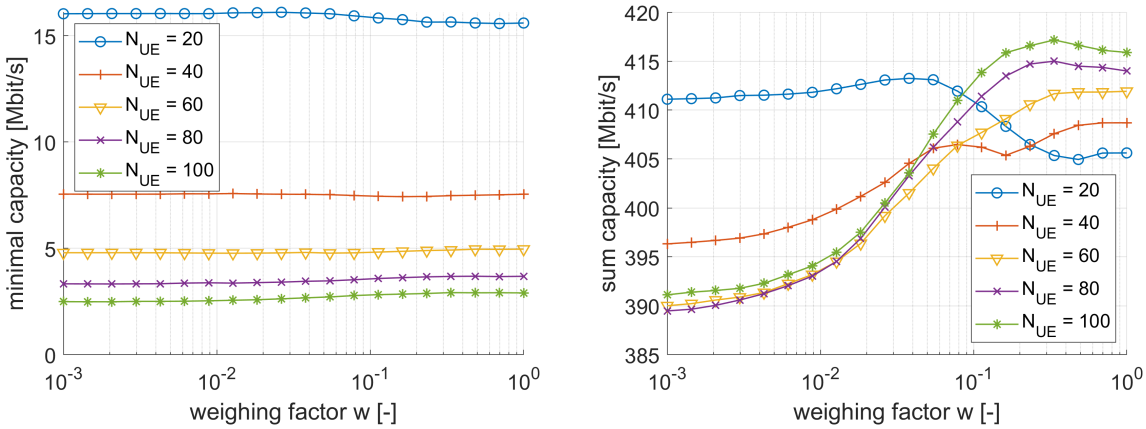

(a) minimal capacity (b) sum capacity

Figure 4.7: Channel capacity depending on weighing factor w, maximal initial positioning step $\alpha_{init} = 50$ m, positioning precision $\epsilon = 0.05$

Consequently, Figure 4.8 illustrates the dependencies of the algorithm complexity on weighing factor w. The number of positioning iterations shown in Figure 4.8a demonstrates the positioning complexity increase with decreasing weight w for higher numbers of UEs in the cell. This is due to the same reason as for the above-described sum capacity decrease. As the less loaded FlyBS reaches the BS bottleneck position while still not fully utilizing its power resources, the net force causes the FlyBS to oscillate around the BS until its positioning step α_j is lower than or equal to 1. In a real network, this behavior may not be that inconvenient, as the FlyBS stationed at the BS could for example recharge. However, it does significantly increase the positioning complexity.

Then, in Figure 4.8b, the association iteration count dependence on the weighing factor is shown. For each of the examined UE numbers, an iteration count minimum is observed. It marks the weighing factor value, for which the least of the UEs are reassociated after the initial association. With increasing UE count, this minimum shifts to higher w values. This is due to the following reason. As the initial association is determined via UE clustering based on distances, with increasing UE count and constant number of FlyBSs,

a lower number of UEs are initially associated with the FlyBSs. This is inconvenient as the FlyBS power resources are then not utilized sufficiently compared to the case with a lower number of UEs in the cell. Therefore, a higher weighing factor for higher UE counts is more satisfactory in terms of subsequent reassociation complexity. However, note that as the reassociation technique is simplified and not optimal, the complexity of the bottleneck elimination does not correlate with the final sum capacity.

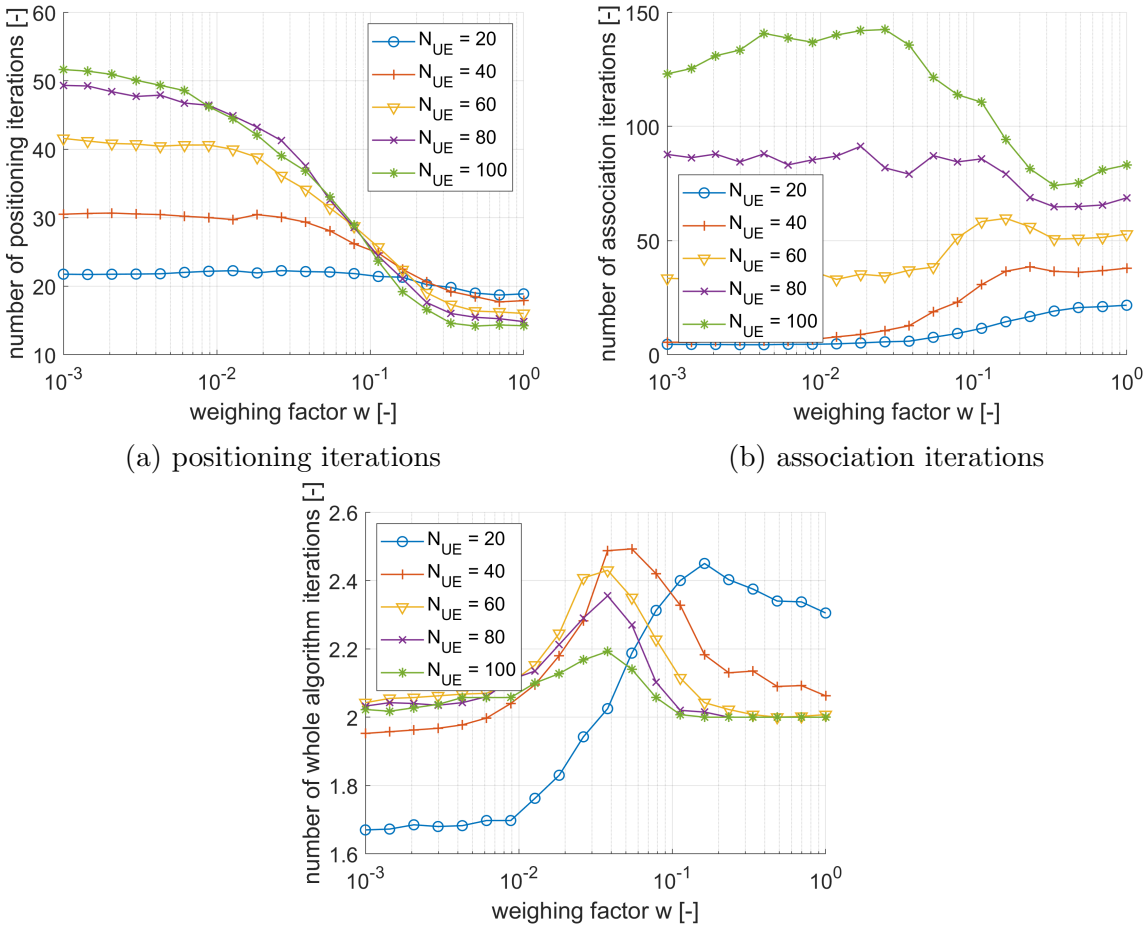

(a) positioning iterations

(b) association iterations

(c) whole algorithm iterations

Figure 4.8: Number of algorithm iterations depending on weighing factor w, maximal initial positioning step $\alpha_{init} = 50$ m, positioning precision $\epsilon = 0.05$

Finally, the whole algorithm iteration count dependence shown in Figure 4.8c confirms the assumptions about the effect of initial FlyBS positioning formulated according to Figure 4.7b. That is, the whole algorithm iteration count is lower for both higher and lower values of weighing factor w, as the FlyBS initially converges either towards the associated UEs or the BS. This way, the FlyBS limits the set of advantageous options for subsequent reassociations, and thus, the algorithm converges earlier. This again does not fully apply for $N_{UE} = 20$, as for higher values of w a really low number of UEs is directly associated with the BS. Therefore, the BS allocates more power for the backhaul links

and does not pull the FlyBSs that close.

To conclude the complexity discussion, only higher UE counts are considered due to the following reasons. Firstly, both algorithm complexity and capacity perform differently for individual numbers of UEs, and thus, it is not possible to choose a common weighing factor that satisfies all UE count scenarios. Secondly, in a real network, deployment of a lower number of FlyBSs to serve a higher number of UEs is expected due to economical reasons. Moreover, the higher UE count is much more sensitive to significant complexity increase. Hence, it is more convenient to determine the final value w with this in mind. Then, based on the discussed capacity and iteration count results, the final weighing factor value is set as $w = 2 \cdot 10^{-1} = 0.2$. This concludes the whole parameterization analysis. The values determined for individual parameters and thus subsequently used for the final performance evaluation are summarized in Table 4.5.

Table 4.5: Overview of the final determined parameterization

parameter	**value**
positioning precision ϵ	0.01
maximal positioning step α_{init}	200 m
weighing factor w	0.2

4.3 Comparison with the competitive schemes

The final performance of the proposed scheme is evaluated based on three quantities. First of them is the minimal capacity among active UEs in the cell, as the objective of this work is to maximize its value. Then, the ability of the proposed power allocation to equalize the channel capacity among UEs is evaluated via the standard deviation of the capacity. Finally, to illustrate how the solution stands in overall throughput performance compared to the competitive schemes, the sum capacity results are presented. All of the introduced key quantities are evaluated depending on both the number of UEs in the cell and the number of deployed FlyBSs. Note that for varying UE count, the number of FlyBSs is fixed at $N_{FlyBS} = 6$. On the contrary, a constant value of $N_{UE} = 50$ UEs is present in the case of the varying number of utilized FlyBSs.

Let's start with the most important quantity, the minimal capacity. Results of all three examined schemes, that is the proposal, k-means, and the backhaul-aware scheme, are presented in Figure 4.9. In Figure 4.9a a gradual decrease in the minimal capacity with the increasing number of UEs in the cell is observed for all of the schemes. This is due to the limited power resources of the cell being divided among the increasing number

of individual UEs. Thus, for higher UE counts, a lower average capacity is observed and the minimal capacity naturally decreases with the average. Note that the minimal capacity reaches much higher values in the case of the proposal compared to both of the competitive schemes. This is due to a much better distribution of the total transmission power among individual links in the cell, which favors the ones with lower channel quality, thus increasing the minimal capacity. On the contrary, both of the competitive schemes neglect those links in terms of power allocation. However, the backhaul-aware scheme still performs better than the k-means, as only the closest UEs are associated with a given FlyBS, while in the case of the k-means the FlyBS is forced to serve the majority of the cluster no matter the distances.

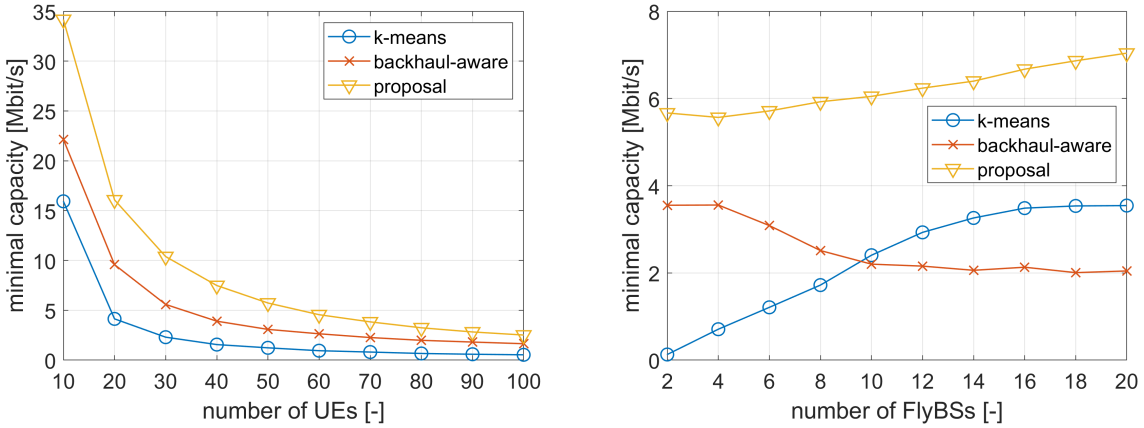

(a) UE count dependence, $N_{FlyBS} = 6$ (b) FlyBS count dependence, $N_{UE} = 50$

Figure 4.9: Minimal channel capacity depending on the number of UEs and FlyBSs, comparison with competitive schemes

In Figure 4.9b, the minimal capacity depending on the varying number of FlyBSs is illustrated for all of the schemes. The proposal's minimal capacity increases with the higher number of deployed FlyBSs. This is due to the fact that the higher FlyBS counts introduce additional power resources to the cell, and thus, the links with low channel quality are allocated more power, increasing the minimal capacity. Similar behavior is observed also in case of the k-means, as the higher density of FlyBSs in the cell area increases the access capacities. However, the k-means' minimal capacity saturates at around $N_{FlyBS} = 16$, as the FlyBSs are that close to the associated UEs, that the bottleneck is shifted from the access to the backhaul.

Nevertheless, in the case of the backhaul-aware scheme, the situation is quite different. As illustrated in Figure 4.9b, the minimal capacity decreases towards higher numbers of UEs until it saturates at around $N_{FlyBS} = 12$. This is due to the fact that the backhaul-aware scheme suffers from very low FlyBS utilization at high FlyBS to UE count ratios. There are two reasons for this. Firstly, the FlyBS allocates transmission powers so that

the capacity on the access link matches the backhaul capacity. However, if the backhaul link is demanding and all UEs are too far from the FlyBS, it might not have enough resources to serve any of them at all, and thus remain fully unutilized. This situation is much more probable for higher FlyBS counts, as the initial positioning of the backhaul-aware scheme is evaluated via k-means clustering, which with decreasing density of UEs per cluster results in fewer of them being stationed close to the centroid. Secondly, for high FlyBS counts, the same k-means behavior might result in the FlyBS being stationed so far from the BS, that associating the UE with the FlyBS is not beneficial compared to the direct association with the BS. This is especially true in the case of only two UEs in a single cluster. Then, the saturation at around $N_{FlyBS} = 12$ is caused by most of the FlyBSs being unutilized.

As illustrated by Figure 4.9, the proposed solution significantly outperforms both of the competitive schemes in terms of the minimal capacity maximization. In the case of the lower FlyBS count, the proposal provides minimal capacity increase compared to the backhaul-aware scheme by approximately 53% – 67% for higher and lower UE counts, while in the case of an average number of UEs the increase reaches up to almost 91%. In case of the k-means, the superiority of the proposal is much more significant, as it outperforms the scheme by 114% – 398% depending on the UE count. Then, in the case of a higher number of deployed FlyBSs, the proposal outperforms both of the competitive schemes by up to almost 244%.

Figure 4.10 shows the channel capacity standard deviation among all UEs in the cell and illustrates the second benefit of the proposed solution. In Figure 4.10a showing the dependence on the number of UEs, the standard deviation decreases with higher UE counts for all of the examined schemes. In the case of both competitive schemes, the capacity deviation is proportional to deviations among distances between UEs and their respective serving stations. These distances can be lowered to a certain degree via the deployment of the FlyBSs. This is the reason why the capacity standard deviation decreases with the increasing UE count of all the presented schemes, as more of the UEs are served by the FlyBSs. However, the standard deviation of the proposal is much lower than for both of the competitive schemes. To explain this, note that the standard deviation among UEs is caused entirely by the path loss prediction, as the virtualized algorithm execution is based on channel gain values burdened with prediction error, contrary to the values used for evaluation of the final results. Therefore, given that no prediction would be used, the capacity standard deviation would actually be zero for all of the UE and FlyBS counts.

To explain the proposal's deviation increase with increasing FlyBS count observed in Figure 4.10b, note that the predicted values are used only for FlyBS-related channels. This

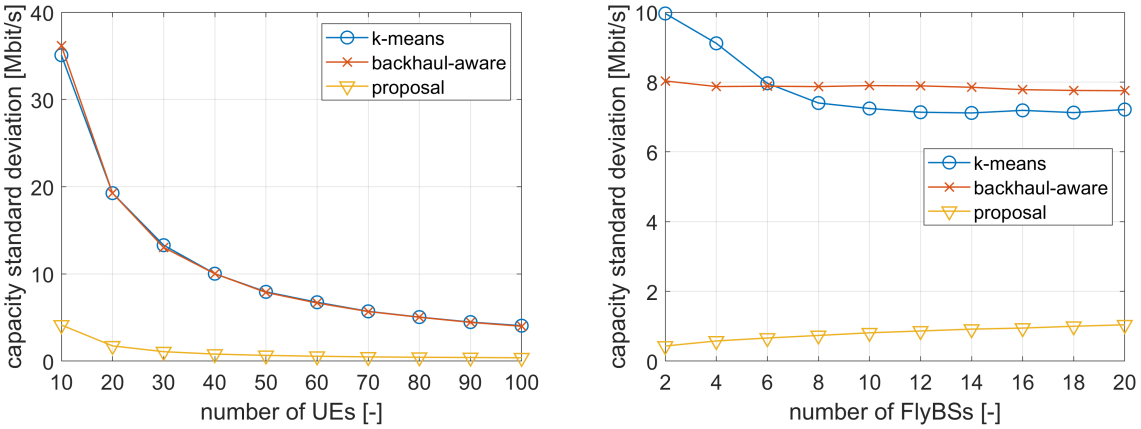

(a) UE count dependence, $N_{FlyBS} = 6$ (b) FlyBS count dependence, $N_{UE} = 50$

Figure 4.10: Channel capacity standard deviation depending on the number of UEs and FlyBSs, comparison with competitive schemes

is due to the fact that the only actual positions that are unknown during the execution of the algorithm are those of the FlyBSs. That is, only the UEs associated with the FlyBSs experience the capacity deviation, while the capacities of all UEs directly associated with the BS are truly equal. Then, as more of the FlyBSs are deployed in the cell, more of the UEs are associated with them, and thus the overall standard deviation increases. However, both backhaul-aware and k-means schemes perform quite differently compared to the UE count dependence. The standard deviation of the backhaul-aware scheme very slightly decreases with the increasing FlyBS count, which is due to the same behavior of the minimal capacity. That is, the decrease in all of the capacities in the system caused by lower FlyBS utilization naturally implies the decrease in the capacity standard deviation. As for the k-means algorithm, the standard deviation is quite high for lower FlyBS counts, and then, it decreases with the increasing number of FlyBSs, until it saturates at around $N_{FlyBS} = 10$. This is due to low FlyBS density at lower FlyBS counts, as also the distant UEs are forced to associate with the FlyBSs. This does not apply for FlyBS counts higher than 10, as the FlyBS density is sufficient to prevent association with the distant UEs. Note that the point of saturation is proportional to the total number of UEs in the cell.

Examining both the UE and FlyBS dependencies, it is apparent that the proposed scheme is superior to both of the competitive schemes in terms of standard deviation minimization, and thus equalization of the capacities among UEs. For all of the UE counts, the proposal performs better by approximately 775% – 1150% compared to both of the competitive schemes. Then, the proposal's standard deviation is approximately 7x – 9x lower in case of higher FlyBS counts, while for lower numbers of FlyBSs the proposal outperforms the other tho schemes by up to almost 1800% in terms of capacity equalization, despite the effect of the channel gain prediction error.

Finally, to examine the overall performance of the proposed solution compared to the competitive schemes, the sum capacity depending on the number of UEs and FlyBSs is analyzed. In Figure 4.11a, a gradual decrease in the sum capacity with the increasing number of UEs in the cell is observed in the case of the proposal. This is due to the effect of initial positioning described in Section 4.2. Let's consider a scenario where a certain FlyBS is initially positioned right above the BS, as a result of the BS serving the majority of the UEs in the cell, and thus acting as a deep bottleneck. As the FlyBS most probably isn't fully utilized, otherwise it would not be allowed to take such a position, it is able to serve more UEs and thus represents a reasonable reassociation target. However, as the FlyBS hovers right above the BS, any of the UEs served by the BS bottleneck can be reassociated to the FlyBS. This may result in the FlyBS serving multiple UEs in various directions from the BS, which is a major problem. The positioning force introduced by the BS is almost zero, and thus, the FlyBS is "torn" by the UE forces, not able to relocate far from the BS. Then, a capacity decrease is observed, as the FlyBS is not able to provide its flexibility and only serves as a power enhancement of the BS. The described phenomenon is much more probable, when more UEs per one FlyBS are present in the cell, as then, a greater portion of them is initially associated with the BS. This explains the gradual decrease of sum capacity with increasing UE count. Additionally, this behavior also represents a non-negligible drawback of the proposed scheme, and as such should be addressed in future works.

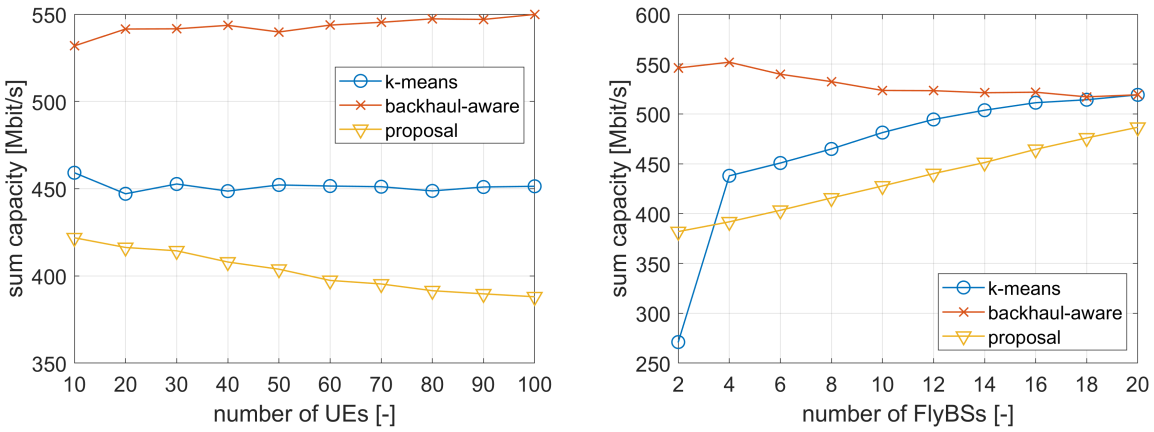

(a) UE count dependence, $N_{FlyBS} = 6$ (b) FlyBS count dependence, $N_{UE} = 50$

Figure 4.11: Sum channel capacity depending on the number of UEs and FlyBSs, comparison with competitive schemes

As illustrated in Figure 4.11a, the sum capacity of both competitive schemes stays approximately the same for all UE counts, although the capacity of the backhaul-aware scheme slightly increases towards higher numbers of UEs. This is again due to the low FlyBS utilization at lower UE counts described according to the minimal capacity. That

is, the lower UE count results in a lower density of UEs in each initial positioning cluster, and thus, fewer of the UEs are stationed close to the centroid, decreasing the probability that any of them is associated with the FlyBS. However, the same does not apply to the sole k-means scheme, as the majority of the cluster is always associated with the FlyBS. Hence, the FlyBSs are always utilized.

The sum capacity dependence on the number of FlyBSs shown in Figure 4.11b resembles the similar behavior for both the proposal and backhaul-aware schemes as described according to the UE count dependence. The only exception is the opposite effect of the FlyBS count increase, which on the contrary decreases the number of UEs per one FlyBS. Therefore, the sum capacity of the proposal increases, as fewer FlyBSs are being pulled above the BS, and at the same time, the backhaul-aware capacity decreases, as the smaller UE clusters result in fewer FlyBS association options and thus decrease the number of utilized FlyBSs. The only difference in the dependence is observed for the k-means, where the sum capacity increases very steeply up to $N_{FlyBS} = 4$, after which the increase is comparable to the proposal. This is due to the fact that the BS serves only those UEs, which are closer to the BS than their initial FlyBS determined via k-means clustering. Then, with the increasing number of FlyBSs, and thus also k-means clusters, more of the UEs are associated with the much more power-supplied BS, resulting in higher sum capacity. This effect is most apparent for the scenario of $N_{FlyBS} = 2$, where the two k-means cluster centroids are much closer to the BS compared to higher FlyBS counts. Then, the majority of the UEs are associated with the FlyBSs and the BS remains heavily unutilized.

All in all, from the sum capacity results, it is apparent that the proposed scheme performs perceptibly worse than both of the competitive schemes in terms of the overall throughput. That is, compared to the backhaul-aware, approximately 25% – 30% worse for lower FlyBS to UE count ratios, and approximately 5% – 17% worse for higher FlyBS to UE count ratios. However, this is in fact only due to the different utilized power allocation schemes, as in the case of the FlyBS-less scenario the proposal shows approximately 40% sum capacity decrease compared to both backhaul-aware and k-means schemes. To explain this, note that the common capacity obtained via the proposed power allocation scheme is given by the power allocation bottleneck. Let's consider a scenario, where the majority of the UEs are positioned closer to the BS, while one or two of the UEs are very distant. Then, utilizing the proposed power allocation scheme to equalize the capacities among all UEs, most of the BS power resources are consumed by the distant UEs and a much lower amount of resources remains to serve the closer ones. Therefore, the overall sum capacity decreases. This is a major trade-off of the capacity equalization via power allocation. However, it is admissible as maximization of the sum capacity is not an objective of this thesis. On the contrary, consider that all of the UEs would be allocated the same

transmission power. Then, the capacities of the distant UEs would be really low. However, as these present only a small portion of the UEs in the cell, their impact on the overall average or sum capacity is minimal.

4.4 Analysis of the multihop utilization

In this section, the results of the simplified multihop scenario simulation are presented and discussed. In order to illustrate the benefits introduced by the multihop utilization, the resulting sum capacities are normalized by capacity values of a simple relay via a single FlyBS, and thus denoted as multihop capacity gain. Results of the multihop simulation are shown in Figure 4.12. As illustrated in Figure 4.12a, the multihop capacity gain for frequency 3.5 GHz only decreases with the increasing number of FlyBSs. This applies to all examined distances R. The reason for this is the interference among individual FlyBS relays, as all of the multihop links use the same spectral resources. Note that the transmitted signal magnitude decreases exponentially with the covered distance according to (2.5). Hence, the SINR depends on both the frequency and distances to the signal sources. If the interference isn't attenuated enough compared to the desired signal, that is, the SINR is lower, a decrease in capacity is observed. This is exactly the case of lower frequency dependence shown Figure 4.12a. The capacity decreases due to the gradual shortening of distances between individual objects forming the multihop relay, and thus the increasing effect of interference. In order to truly utilize the multihop, a higher distance to cover R is required. This is indicated by the multihop gain for $R = 400$ m, where the multihop relay formed by 2 FlyBSs does not result in a capacity loss.

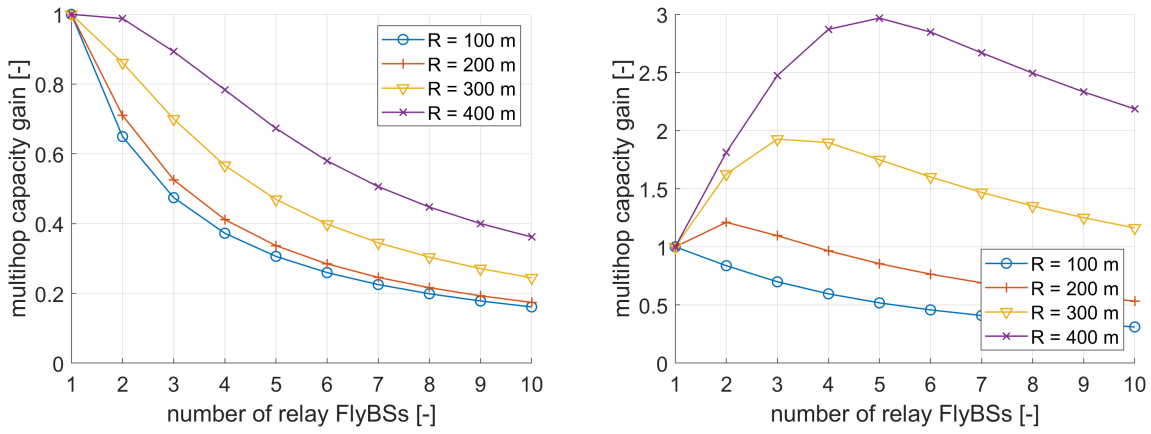

(a) carrier frequency 3.5 GHz

(b) carrier frequency 39 GHz

Figure 4.12: Multihop capacity gain depending on the number of FlyBSs N_{FlyBS}, distances R_T and carrier frequencies f

On the contrary, Figure 4.12b illustrates the true benefit of the multihop via utilizing a much higher, millimeter-wave band frequency. Given a specific distance R, the multihop gain increases towards a certain FlyBS count, after which a gradual decrease is observed. This is due to the increasing effect of interference, as the mutual distances between individual multihop objects shorten. The cutoff FlyBS count, at which a multihop gain maximum is observed and thus denotes the highest performing multihop degree, is proportional to both f and R. Then, note that for lower frequencies or distances, the cutoff FlyBS count may not be present at all, as the interference results in capacity gain decrease already for multihop degree 2, as illustrated by Figure 4.12a and distance $R = 100$ m in Figure 4.12b. In such a case, the cutoff FlyBS count in fact corresponds to the multihop degree less than or equal to 1, and thus, deployment of the multihop does not prove beneficial. Nevertheless, based on both Figures 4.12a and 4.12b, it is concluded that the multihop deployment is beneficial especially for higher frequencies.

Chapter 5

Conclusion

The objective of this thesis was to maximize the minimal channel capacity among individual users within the mobile network supported by FlyBSs, and thus provide reliable connectivity to every UE during a general emergency scenario, where securing sufficient capacity is critical for search and rescue. To this end, a joint solution that finds positions of deployed FlyBSs, determines associations of UEs, and allocates transmission powers to all of the links within the cell has been proposed. First, a system model describing the considered network has been established and the addressed minimal capacity maximization problem formulated. Then, the defined problem has been divided into three simplified subproblems and each solved separately. Consequently, the individual solutions have been combined into a final framework providing a definitive joint configuration.

The introduced power allocation scheme distributes the available transmission power among all of the links within the cell so that every UE experiences the same end-to-end channel capacity. This way the proposed solution secures the minimal capacity maximization while utilizing only the power resources necessary. The scheme is then adopted by UE association and FlyBS positioning algorithms that balance and improve the whole system's resource utilization and thus further boost the common channel capacity. Finally, the overall framework is implemented as a joint algorithm that alternately reassociates the UEs and repositions the FlyBSs, until a state of convergence is achieved after several iterations.

Following the described solution proposal, an analysis of the designed algorithms' parameterization has been conducted via a series of simulations, resulting in the determination of the framework's final settings. In the end, the performance of the final solution, challenged by two additional competitive schemes, has been evaluated based on various scenarios. The results demonstrate that the proposal significantly outperforms both of the compared schemes in terms of minimal capacity maximization, and that is by approximately 53% – 91% in the case of a lower number of deployed FlyBSs, which is more

expected in a real network due to economical reasons. Then, for higher FlyBS counts, the results show a much higher increase by up to almost 244% compared to the competitive schemes. However, this is achieved at the cost of the sum capacity, where a non-negligible decrease of approximately 5% – 30% is observed based on the total number of UEs and FlyBSs in the cell. Nonetheless, despite the sum capacity trade-off, the overall results are highly favorable, as the minimal capacity increase would significantly contribute to maintaining reliable connectivity with all of the critical users during an emergency scenario.

In addition, the possibility of the FlyBS multihop integration has been examined based on a simplified scenario, where all of the links are allocated the same power resources. The results of the simulation show that the multihop deployment is beneficial only for higher carrier frequencies, as otherwise, the interference among individual hops of the relay results in a capacity decrease. Moreover, due to the same reason, only a limited number of FlyBSs, proportional to both the frequency and the distance to cover, can be deployed for the multihop to be beneficial.

In future research, a proper multihop integration in the proposed framework should be addressed. This is an important aspect as the proposed scheme considers only a scenario, where the reference cell BS is working. However, in a real emergency situation, the BS serving the critical area may be damaged. Therefore, the multihop would not only enable a coverage increase but also provide a relay bridge to forward communication of the damaged cell to a neighboring BS. Additionally, the UE association should be improved to prevent lower FlyBS utilization observed in some scenarios, and thus, increase the overall throughput of the cell. Finally, to support a real-time utilization of the proposed scheme, possibilities of the framework optimization should be studied. Regarding this, primarily machine learning represents a promising means of efficient association and power allocation evaluation, where specifically a deep neural network could be used to lower computational complexity or determine whether a certain reassociation would be beneficial.

Appendix A

Attachments

To this thesis, all MATLAB projects used for simulation of the proposed solution and the competitive schemes are attached. The list of the projects is summarized in Table A.1.

Table A.1: List of attached MATLAB projects

project name	**description**
proposal_simulation_analysis_pos_step	proposed scheme's maximal initial positioning step α_{init} analysis simulation
proposal_simulation_analysis_pos_prec	proposed scheme's positioning precision ϵ analysis simulation
proposal_simulation_analysis_weight	proposed scheme's weighing factor w analysis simulation
proposal_simulation_final	simulation of the proposed scheme for final perfomance evaluation
backhaul_aware_simulation	simulation of the backhaul-aware competitive scheme for perfomance evaluation
kmeans_simulation	simulation of the k-means competitive scheme for perfomance evaluation
multihop_simulation	simulation of the multihop scenario

Each of the above listed MATLAB projects is structured in the following way:

- **Main simulation M-file** – This is the main source file defining the simulation structure and via which the simulation is executed. Multiple main source files may be present in a single project, each providing simulation based on different varying parameters, e.g., number of UEs or FlyBSs.

- **Functions** – Simple routines that serve as fundamental blocks of the simulation's logical structure. They are used for the evaluation and determination of the system model's quantities, such as channel gain, channel capacity, positions of network objects, etc.

- **Classes** – A total of five classes are implemented to define individual network object types and the simulated RAN environment. In the case of the proposed scheme, the RAN class provides the implementation of most of the designed algorithms and functionalities.

- **Results** – A directory containing all the simulation results, that is, numerical values both stored in respective TXT files and plotted in MATLAB figures and PNG files.

- **UE position TXT file** – A file containing randomly generated positions of the UEs for every drop of the simulation.

Note that for execution of most of the simulation projects the MATLAB Parallel Computing Toolbox is required [31].

References

[1] A. Mourad, R. Yang, P. H. Lehne, and A. de la Oliva, "Towards 6G: Evolution of Key Performance Indicators and Technology Trends", in *2020 2nd 6G Wireless Summit (6G SUMMIT)*, 2020, pp. 1–5. DOI: 10.1109/6GSUMMIT49458.2020.9083759.

[2] Y. Wang, J. Li, L. Huang, Y. Jing, A. Georgakopoulos, and P. Demestichas, "5G Mobile: Spectrum Broadening to Higher-Frequency Bands to Support High Data Rates", *IEEE Vehicular Technology Magazine*, vol. 9, no. 3, pp. 39–46, 2014, ISSN: 1556-6080. DOI: 10.1109/MVT.2014.2333694.

[3] T. S. Rappaport, Y. Xing, G. R. MacCartney, A. F. Molisch, E. Mellios, and J. Zhang, "Overview of Millimeter Wave Communications for Fifth-Generation (5G) Wireless Networks—With a Focus on Propagation Models", *IEEE Transactions on Antennas and Propagation*, vol. 65, no. 12, pp. 6213–6230, 2017, ISSN: 1558-2221. DOI: 10.1109/TAP.2017.2734243.

[4] M. Giordani, A. Zanella, and M. Zorzi, "Millimeter wave communication in vehicular networks: Challenges and opportunities", in *2017 6th International Conference on Modern Circuits and Systems Technologies (MOCAST)*, 2017, pp. 1–6. DOI: 10.1109/MOCAST.2017.7937682.

[5] Z. Becvar, M. Vondra, P. Mach, J. Plachy, and D. Gesbert, "Performance of Mobile Networks with UAVs: Can Flying Base Stations Substitute Ultra-Dense Small Cells?", in *European Wireless 2017; 23th European Wireless Conference*, 2017, pp. 1–7.

[6] V. Sharma, K. Srinivasan, H.-C. Chao, K.-L. Hua, and W.-H. Cheng, "Intelligent deployment of UAVs in 5G heterogeneous communication environment for improved coverage", *Journal of Network and Computer Applications*, vol. 85, pp. 94–105, 2017, Intelligent Systems for Heterogeneous Networks, ISSN: 1084-8045. DOI: https://doi.org/10.1016/j.jnca.2016.12.012. [Online]. Available: https://www.sciencedirect.com/science/article/pii/S1084804516303034.

[7] S. A. Al-Ahmed, M. Z. Shakir, and S. A. R. Zaidi, "Optimal 3D UAV base station placement by considering autonomous coverage hole detection, wireless backhaul and user demand", *Journal of Communications and Networks*, vol. 22, no. 6, pp. 467–475, 2020, ISSN: 1976-5541. DOI: 10.23919/JCN.2020.000034.

[8] Y. Liu, W. Huangfu, H. Zhou, H. Zhang, J. Liu, and K. Long, "Fair and Energy-efficient Coverage Optimization for UAV Placement Problem in the Cellular Network", *IEEE Transactions on Communications*, pp. 1–1, 2022, ISSN: 1558-0857. DOI: 10.1109/TCOMM.2022.3170615.

[9] W. Guo, C. Devine, and S. Wang, "Performance analysis of micro unmanned airborne communication relays for cellular networks", in *2014 9th International Symposium on Communication Systems, Networks Digital Sign (CSNDSP)*, 2014, pp. 658–663. DOI: 10.1109/CSNDSP.2014.6923909.

[10] S. Rohde and C. Wietfeld, "Interference Aware Positioning of Aerial Relays for Cell Overload and Outage Compensation", in *2012 IEEE Vehicular Technology Conference (VTC Fall)*, 2012, pp. 1–5. DOI: 10.1109/VTCFall.2012.6399121.

[11] G. Li, C. Zhuang, Q. Wang, Y. Li, X. Xu, and W. Zhou, "A UAV Real-time Trajectory Optimized Strategy for Moving Users", in *2019 11th International Conference on Wireless Communications and Signal Processing (WCSP)*, 2019, pp. 1–6. DOI: 10.1109/WCSP.2019.8927863.

[12] R. Grodi and D. B. Rawat, "UAV-assisted broadband network for emergency and public safety communications", in *2015 IEEE Global Conference on Signal and Information Processing (GlobalSIP)*, 2015, pp. 10–14. DOI: 10.1109/GlobalSIP.2015.7416926.

[13] M. Mozaffari, W. Saad, M. Bennis, Y.-H. Nam, and M. Debbah, "A Tutorial on UAVs for Wireless Networks: Applications, Challenges, and Open Problems", *IEEE Communications Surveys Tutorials*, vol. 21, no. 3, pp. 2334–2360, 2019, ISSN: 1553-877X. DOI: 10.1109/COMST.2019.2902862.

[14] X. Zhong, Y. Guo, N. Li, and Y. Chen, "Joint Optimization of Relay Deployment, Channel Allocation, and Relay Assignment for UAVs-Aided D2D Networks", *IEEE/ACM Transactions on Networking*, vol. 28, no. 2, pp. 804–817, 2020, ISSN: 1558-2566. DOI: 10.1109/TNET.2020.2970744.

[15] X. Zhong, Y. Guo, N. Li, and S. Li, "Deployment Optimization of UAV Relays for Collecting Data From Sensors: A Potential Game Approach", *IEEE Access*, vol. 7, pp. 182 962–182 973, 2019, ISSN: 2169-3536. DOI: 10.1109/ACCESS.2019.2960314.

[16] H. El Hammouti, M. Benjillali, B. Shihada, and M.-S. Alouini, "A Distributed Mechanism for Joint 3D Placement and User Association in UAV-Assisted Networks", in *2019 IEEE Wireless Communications and Networking Conference (WCNC)*, 2019, pp. 1–6. DOI: 10.1109/WCNC.2019.8885539.

[17] X. Xi, X. Cao, P. Yang, J. Chen, T. Quek, and D. Wu, "Joint User Association and UAV Location Optimization for UAV-Aided Communications", *IEEE Wireless Communications Letters*, vol. 8, no. 6, pp. 1688–1691, 2019, ISSN: 2162-2345. DOI: 10.1109/LWC.2019.2937077.

[18] J. Plachy, Z. Becvar, P. Mach, R. Marik, and M. Vondra, "Joint Positioning of Flying Base Stations and Association of Users: Evolutionary-Based Approach", *IEEE Access*, vol. 7, pp. 11 454–11 463, 2019, ISSN: 2169-3536. DOI: 10.1109/ACCESS.2019.2892564.

[19] A. Fouda, A. S. Ibrahim, Güvenç, and M. Ghosh, "Interference Management in UAV-Assisted Integrated Access and Backhaul Cellular Networks", *IEEE Access*, vol. 7, pp. 104 553–104 566, 2019, ISSN: 2169-3536. DOI: 10.1109/ACCESS.2019.2927176.

[20] P. Mach, Z. Becvar, and M. Najla, "Joint Association, Transmission Power Allocation and Positioning of Flying Base Stations Considering Limited Backhaul", in *2020 IEEE 92nd Vehicular Technology Conference (VTC2020-Fall)*, 2020, pp. 1–7. DOI: 10.1109/VTC2020-Fall49728.2020.9348784.

[21] J. Plachy and Z. Becvar, "Energy Efficient Positioning of Flying Base Stations via Coulomb's law", in *2020 IEEE Globecom Workshops (GC Wkshps)*, 2020, pp. 1–6. DOI: 10.1109/GCWkshps50303.2020.9367495.

[22] M. Deruyck, J. Wyckmans, and W. Joseph, "Designing UAV-aided emergency networks for large-scale disaster scenarios", in *EURASIP Journal on Wireless Communications and Networking*, 2018. DOI: 10.1186/s13638-018-1091-8.

[23] N. Zhao, W. Lu, M. Sheng, *et al.*, "UAV-Assisted Emergency Networks in Disasters", *IEEE Wireless Communications*, vol. 26, no. 1, pp. 45–51, 2019, ISSN: 1558-0687. DOI: 10.1109/MWC.2018.1800160.

[24] Z. Yao, W. Cheng, W. Zhang, and H. Zhang, "Resource Allocation for 5G-UAV-Based Emergency Wireless Communications", *IEEE Journal on Selected Areas in Communications*, vol. 39, no. 11, pp. 3395–3410, 2021, ISSN: 1558-0008. DOI: 10.1109/JSAC.2021.3088684.

[25] U. Siddique, H. Tabassum, E. Hossain, and D. I. Kim, "Wireless backhauling of 5G small cells: Challenges and solution approaches", *IEEE Wireless Communications*, vol. 22, no. 5, pp. 22–31, 2015, ISSN: 1558-0687. DOI: 10.1109/MWC.2015.7306534.

[26] P. Mach, Z. Becvar, and M. Najla, "Power Allocation, Channel Reuse, and Positioning of Flying Base Stations With Realistic Backhaul", *IEEE Internet of Things Journal*, vol. 9, no. 3, pp. 1790–1805, 2022, ISSN: 2327-4662. DOI: 10.1109/JIOT.2021.3088287.

[27] M. Najla, Z. Becvar, P. Mach, and D. Gesbert, "Predicting Device-to-Device Channels from Cellular Channel Measurements: A Learning Approach", vol. 19, no. 11, pp. 7124 –7138, 2020, ISSN: 1536-1276.

[28] M. Najla, Z. Becvar, P. Mach, and D. Gesbert, "Positioning and Association Rules for Transparent Flying Relay Stations", vol. 10, no. 6, pp. 1276–1280, 2021, ISSN: 2162-2337.

[29] R. Xu and D. Wunsch, "Survey of clustering algorithms", *IEEE Transactions on Neural Networks*, vol. 16, no. 3, pp. 645–678, 2005, ISSN: 1941-0093. DOI: 10.1109/TNN.2005.845141.

[30] "NR; User Equipment (UE) radio transmission and reception; part 2: Range 2 Standalone (Release 17)", 3rd Generation Partnership Project, Valbonne, France, Standard 3GPP TS 38.101-2, Mar. 2022. [Online]. Available: https://portal.3gpp.org/desktopmodules/Specifications/SpecificationDetails.aspx?specificationId=3284.

[31] "Parallel Computing Toolbox," MathWorks. [online]. Available: https://www.mathworks.com/products/parallel-computing.html. [Accessed: 18-May-2022].